Summer 2023

U-Pb Zircon Geochronology and Structure of regional blueschist units in the Easton metamorphic suite, Northwest Cascades, WA

Katherine Lang
Western Washington University, klippekatie@gmail.com

U-Pb Zircon Geochronology and Structure of regional blueschist units in the Easton metamorphic suite, Northwest Cascades, WA

By

Katherine E. Lang

Accepted in Partial Completion
Of the Requirements for the Degree
Master of Science

ADVISORY COMMITTEE

Dr. Sean Mulcahy, Chair

Dr. Elizabeth Schermer

Dr. Sarah Roeske

GRADUATE SCHOOL

Dr. David Patrick, Dean

Master's Thesis

In presenting this thesis in partial fulfillment of the requirements for a master's degree at Western Washington University, I grant to Western Washington University the non-exclusive royalty-free right to archive, reproduce, distribute, and display the thesis in any and all forms, including electronic format, via any digital library mechanisms maintained by WWU.

I represent and warrant this is my original work and does not infringe or violate any rights of others. I warrant that I have obtained written permissions from the owner of any third party copyrighted material included in these files.

I acknowledge that I retain ownership rights to the copyright of this work, including but not limited to the right to use all or part of this work in future works, such as articles or books.

Library users are granted permission for individual, research and non-commercial reproduction of this work for educational purposes only. Any further digital posting of this document requires specific permission from the author.

Any copying or publication of this thesis for commercial purposes, or for financial gain, is not allowed without my written permission.

Katherine E. Lang

July 2023

U-Pb Zircon Geochronology and Structure of regional blueschist units in the Easton metamorphic suite, Northwest Cascades, WA

A Thesis
Presented to
The Faculty of
Western Washington University

In Partial Fulfillment
Of the Requirements for the Degree
Master of Science

By
Katherine E. Lang
July 2023

ABSTRACT

The Easton metamorphic suite of the Northwest Cascades Thrust System (NWCS) is a well-preserved subduction accretion complex in Washington State. The regional blueschist units of the Easton metamorphic suite include the Mt. Josephine semi-schist, Darrington Phyllite, and Shuksan greenschist/blueschist and all are interpreted to have accreted after the onset of Jurassic subduction beneath North America. This study uses zircon U-Pb geochronology, structure, and field observations to test the regional correlations between units in the Easton metamorphic suite and address models for the timing of subduction accretion along the North American margin in the Late Jurassic – Early Cretaceous. The results suggest that previously correlative units in the Easton metamorphic suite are instead structurally distinct litho-tectonic units. The Mt. Josephine semi-schist has at least two distinct groups of maximum depositional ages at ~144 Ma and ~122 Ma and suggests different sources within the same unit or that the Mt Josephine semi-schist consists of units accreted at separate times. The Lummi Formation in the NWCS yields similar maximum depositional ages as the older portions of the Mt Josephine semi-schist and may be correlative. The oldest portions of the Mt. Josephine appear to be ~8 m.y. younger than the Darrington phyllite and the youngest Mt. Josephine maximum depositional ages are younger than previously published white mica $^{40}Ar/^{39}Ar$ ages of the Darrington. The Shuksan greenschist has a protolith age of ~166 Ma but the structural and metamorphic history is different from the Darrington phyllite and the two units should be considered separately. The geochronology presented in this study documents an almost complete continuum of zircon ages from the Mid-Jurassic up to ~120 Ma. Deposition and subsequent quick subduction accretion in the Easton metamorphic suite occurred ~30 m.y. earlier than the main accretionary phase in the Franciscan of

California and suggests that proposed changes in relative Pacific - North American plate motion did not solely drive changes from subduction erosion to subduction accretion.

ACKNOWLEDGEMENTS

There are several people who deserve many thanks and gratitude. Firstly, I want to thank my advisor, Dr. Sean Mulcahy, for his generous guidance and unwavering encouragement through all aspects of this work, even when the primary focus of this project changed halfway through. I also thank my other committee members, Dr. Liz Schermer and Dr. Sarah Roeske, who both provided insightful and constructive comments that ensured my research considered all avenues. Thank you to Kalieh Singleton, Grace Sutherland, and Eston Worthington for providing help gathering zircon samples while in the field. Thank you to Ben Paulson for help with lab equipment at WWU and Dr. Mai Sas for her petrology wisdom and general encouragement. Thank you so much to Kate Blizzard who was always more than willing to go over funding and TA forms with me to ensure they were correct. To the entire University of Arizona LaserChron Lab staff who helped show me how to prepare and separate my zircon samples, and for running my U-Pb analyses during the very earliest stages of the pandemic: thank you. Thanks must be given to the previous geologists who have worked in the Easton metamorphic suite – I truly stand on the shoulders of incredible past researchers. I also want to thank my geology graduate cohort for the support during the years at WWU and for the strong comradery that persists even now. Thank you to my colleagues at the Virginia Energy Geology and Mineral Resources Program for constantly cheering me on. Finally, I want to thank my parents for their steadfast support from the opposite side of the country. A special thanks goes to my late father who battled stage 4 pancreatic cancer throughout my time in graduate school and who was always so supportive of my research regardless of the tough circumstances. This work was supported by funding from the WWU Graduate School, the WWU Department of Geology, the WWU Advanced Materials Science and Engineering Center, the Geological Society of America, and the GSA Structural Geology and Tectonics Division.

TABLE OF CONTENTS

ABSTRACT ..... *iv*

ACKNOWLEDGEMENTS ..... *vi*

LIST OF FIGURES: ..... *ix*

1. INTRODUCTION *1*

2. THE EASTON METAMORPHIC SUITE *3*

2.1 Regional Geology 3

2.2 Lithology of the Regional Blueschist Units 4

2.2.1 Mt. Josephine semi-schist 4

2.2.2 Darrington phyllite 5

2.2.3 Shuksan greenschist 6

2.3 Previous U-Pb Zircon Constraints on Protolith Ages in the Easton metamorphic suite 7

2.4 Competing Early Subduction Accretion Models 7

3. METHODS *9*

3.1 Field, Structural, and Petrographic Methods 9

3.2 U-Pb Zircon Geochronology Methods 10

4. RESULTS *11*

4.1 Lithologic Units, Mineralogy, and Structural Fabrics 11

4.1.1 Mt. Josephine semi-schist 12

4.1.2 Darrington phyllite 13

4.1.3 Observed differences between the Mt. Josephine semi-schist and Darrington phyllite 14

4.1.4 Shuksan greenschist 15

4.2 Zircon U-Pb geochronology results 16

4.2.1 Mt Josephine semi-schist 17

4.2.2 Darrington phyllite 19

4.2.3 Shuksan greenschist 20

5. DISCUSSION *21*

5.1 Age Relationships of the Mt. Josephine, Darrington, and Shuksan units 22

5.2 Correlations Within the Northwest Cascades System 27

5.3 Depositional Environments and Provenance of the Regional Blueschist Units of the EMS 29

5.4 Causes of Subduction Accretion along the North American Margin.....35

6. CONCLUSIONS.....*37*

7. FUTURE WORK.....*37*

REFERENCES CITED.....*39*

LIST OF FIGURES:

FIGURE 1. Geologic map and cross section of the Northwest Cascades Thrust system (NWCS) nappe sequence. 45
FIGURE 2. Easton metamorphic suite diagrams 46
FIGURE 3. Geologic map of the Easton metamorphic suite, with sample locations for this study 47
FIGURE 4. Stereograms of foliation planes in the Blanchard Mountain and Iron Mountain study areas. 48
FIGURE 5. Field photographs of U-Pb zircon geochronology samples 49
FIGURE 6. Field photos of folds 52
FIGURE 7. Thin section photomicrographs of U-Pb geochronology samples. 53
FIGURE 8. Thin section photomicrographs of the Mt. Josephine semi-schist and Darrington phyllite samples 55
FIGURE 9. Thin section photomicrographs of the Shuksan greenschist/blueschist 56
FIGURE 10. Stereonet plot of axial planes. 58
FIGURE 11. Wetherill-Concordia diagrams for samples with a high-N zircon yield. 59
FIGURE 12. Kernel density estimate plots for samples with a high-N zircon yield 60
FIGURE 13. Cumulative age distribution plots for samples with a high-N zircon yield. 62
FIGURE 14. Stacked cumulative age distribution plots and kernel density estimates of the Mt. Josephine detrital samples with a high-N zircon yield 63
FIGURE 15. YC2σ(3+) plots showing the calculated maximum depositional ages for the Mt. Josephine samples with a high-N zircon yield 64
FIGURE 16. Yc2σ(3+) plots showing the calculated maximum depositional ages for samples with a low-N zircon yield 65
FIGURE 17. TuffZirc plot and weighted mean plot of the Shuksan greenschist 66
FIGURE 18. Lithotectonic column of the regional blueschist units. 67
FIGURE 19. Geologic map of the NWCS with new U-Pb geochronology 68
FIGURE 20. Stacked cumulative age distribution and kernel density estimate plot of the Constitution and Lummi Formations, Fidalgo Complex, and Mt. Josephine semi-schist within the NWCS 69

FIGURE 21. YC2σ(3+) plots showing the calculated maximum depositional ages of the Constitution and Lummi Formations, Fidalgo Complex, and Mt. Josephine semi-schist within the NWCS..... 70
FIGURE 22. Comparison of timing of events in the Franciscan subduction complex and the Easton metamorphic suite..... 72

LIST OF TABLES:

TABLE 1. Sample locations, unit names, and lithologies for geochronology samples. 73
TABLE 2. Geochronology samples, zircon yields, reported age types, and ages. 73

1. INTRODUCTION

The Northwest Cascades Thrust System (NWCS) in Washington state is a package of high-pressure low-temperature nappes that preserves a prolonged record of subduction accretion along western North America from ~170 Ma to ~<95 Ma (Fig. 1) (Brown, 1987; Brandon et al., 1988; Brown, 2012; Cordova et al., 2019). The accretion of similar Jurassic-Cretaceous subduction units in North America has been linked to changes in plate motion (Dumitru et al., 2010) and understanding the formation and evolution of units in the NWCS can offer further insight into the processes that control subduction accretion and erosion on the Cordilleran margin. Within the NWCS, the Easton Metamorphic Suite (EMS) is a structurally high nappe (Fig. 1) that preserves the earliest record of subduction initiation and subsequent accretion (Brown et al., 1982, Brown et al., 1986, Cordova et al., 2019). Despite the importance of the EMS to the early subduction history of the NWCS, the spatial extent, age, and structural relationships of the units within the EMS are debated.

The Easton metamorphic suite contains several litho-tectonic units of varied protolith, age, and metamorphic conditions (Fig. 2). The oldest and highest-grade rocks consist of garnet amphibolite, Na-amphibole schist, and serpentinite. Together, these rocks are interpreted to record subduction initiation and subsequent metamorphism between >167-157 Ma (Brown et al., 1982; Cordova et al., 2019). Younger and lower grade regional blueschist units were metamorphosed between 149-137 Ma and occur structurally beneath the older high-grade assemblages (Haugerud et al., 1981; Brown et al., 1982; Cordova et al., 2019). Individual units within the regional blueschist have been separated largely based on different protoliths and include the Mt. Josephine semi-schist, Darrington phyllite, and Shuksan greenschist (Misch, 1966; Haugerud et al., 1981; Brown, 1986; Tabor et al., 2003). Most workers consider the Mt. Josephine semi-schist to be a

coarser-grained equivalent of the Darrington phyllite (e.g., Misch, 1966; Brown et al., 1987; and Tabor et al., 2003), however there are different interpretations for the relationship between the Darrington phyllite and Shuksan greenschist. The first interpretation posits that the regional blueschist facies rocks are a single unit and the Darrington phyllite was deposited as a mudstone on the volcanic protolith of the Shuksan greenschist prior to subduction. This interpretation suggests that the Shuksan is older than the Darrington (Haugerud et al., 1981; Brown et al., 1982). The second interpretation argues that the regional blueschist contains distinct units accreted at different times. This theory argues that the contacts between units are structural and that the Shuksan is younger than the Darrington phyllite (Cordova et al., 2019). Though the southwestern extent of the Easton metamorphic suite already has a well-constrained record of metamorphic ages (e.g. Cordova et al., 2019), a determination of protolith and depositional ages for the Mt. Josephine semi-schist, Darrington phyllite, and Shuksan greenschist is necessary to further understand the subduction history of the region.

In this work, I combine structural analysis and U-Pb zircon geochronology from the Mt. Josephine semi-schist, Darrington phyllite, and Shuksan greenschist in the Easton metamorphic suite to evaluate existing interpretations of the Shuksan greenschist and Darrington phyllite contact, as well as the assumption that the Mt. Josephine semi-schist and the Darrington phyllite are one unit. The new data confirm that the Shuksan greenschist and Darrington phyllite are distinct units and are likely separated by a structural contact. In addition, maximum depositional ages of the Mt. Josephine semi-schist are younger than the depositional age and metamorphic ages of the Darrington phyllite, and likely do not support interpretations that they are the same unit. The results from this work also imply that subduction accretion along the North American margin probably

started earlier than suggested by previous studies that examined correlative subduction complexes south of the NWCS like the Franciscan Complex of California (Brown and Blake, 1987).

2. THE EASTON METAMORPHIC SUITE

2.1 Regional Geology

The Northwest Cascades Thrust System (NWCS) of western Washington (Fig. 1) is a series of northwest verging structural nappes that were thrust over the Coast Plutonic Complex (CPC) and Wrangellia terrane (Brown, 2012). The stacked nappes of the NWCS are composed of Paleozoic to Late-Cretaceous ocean floor, island-arc, and trench deposits (Misch, 1966; Brown et al., 1982; Brown, 2012) that experienced high-pressure, low-temperature metamorphism (Brown et al., 1986). The Easton metamorphic suite (formerly Shuksan nappe or Shuksan terrane), one of the nappes within the NWCS, sits at a high structural position within the nappe sequence and contains a Jurassic-Cretaceous subduction suite that formed during and after the beginning of Farallon plate subduction underneath North America (Cordova et al., 2019). The Easton is unique because it preserves high-grade amphibolite facies rocks interpreted as a metamorphic sole (Fig. 2A) and the lower-grade regional blueschist facies rocks that formed during some of the earliest stages of subduction. Together, the units within the Easton record approximately 30 million years of subduction and accretion from ~167 Ma to ~137 Ma (Brown et al., 1982; Schermer et al., 2007; Cordova et al., 2019). Based on age brackets for the underlying thrust, the Easton Suite was emplaced into its current position within the NWCS after 95 Ma but before 87 Ma (Tabor, 1994; Brown, 2012).

2.2 Lithology of the Regional Blueschist Units

The lithology of units within the EMS is variable; this study focuses on comparing the units in the study areas outlined in Figures 3 and 4. The western portion of the EMS is composed of the Darrington phyllite and the coarser Mt. Josephine semi-schist (blueschist facies meta-sediments) (Fig. 4A), but potentially includes diorite and gabbro of uncertain structural association located in the Blanchard Mountain area. Dragovich et al. (1998) argued that these metaigneous rocks constitute part of the Helena Haystack Mélange, whereas Gallagher et al. (1988) considered these rocks as part of the Shuksan Suite. In this westernmost region of the Easton, the rocks lack evidence of the higher-grade amphibolite facies metamorphism observed in the Iron Mountain area, and only record blueschist-facies metamorphism in the schist, phyllite, and associated low-grade metabasalt and gabbro (Brown et al., 1982). In the southeastern exposures of the study area, between Iron Mountain and Gee Point/Finney Creek (Fig. 4B), serpentinite, amphibolite, and Na-amphibole schist structurally lie above the lower-grade rocks of the regional blueschists that include the Shuksan greenschist/blueschist (blueschist facies metavolcanics) and the Darrington phyllite (blueschist facies pelites) (Fig. 2A-B). Metamorphic temperature decreases structurally downward from around >800˚C to 600-500˚C in the amphibolite and Na- amphibole schist down to ≤350-250˚C in low-temperature regional blueschist units (Brown et al., 1982; Cordova et al., 2019) (Fig. 2A).

2.2.1 Mt. Josephine semi-schist

The Mt. Josephine semi-schist has historically been mapped as a co-eval, coarser-grained sub-unit of the Darrington phyllite within the Easton metamorphic suite (Dragovich et al., 1998; Dragovich et al., 2000; and Tabor et al., 2003). The Mt. Josephine semi-schist commonly occurs

as a semi-schistose metagraywacke that is gray to dark gray to beige in color. The unit varies from fine- to medium- grained and primarily contains varying amounts of quartz, albite, and phengitic to sericitic white-mica as the most abundant minerals, with minor amounts of actinolite, chlorite, and epidote in addition to lithic fragments. According to Gallagher et al. (1988) the lithic clasts consist of intermediate to felsic volcanic rocks, metachert, and gabbro/diorite in decreasing order, with some attenuated clasts up to 60 cm in length. In contrast, Dragovich et al. (1998) argued that meta-chert clasts were more common in the Mt. Josephine semi-schist, not volcanic clasts like Gallagher et al. (1988) first suggested. However, Gallagher primarily focused on the rocks adjacent to the mafic rocks on Blanchard Mountain, whereas Dragovich worked on a larger extent of the semi-schist.

The differences outlined between the Mt. Josephine semi-schist and the Darrington phyllite are based predominantly upon grain size and lithology of the clasts. The contacts between the two units have often been described as gradational and intercalated. Because of the general similarities, some researchers do not classify the Darrington and the Mt. Josephine as separate rock units (e.g., Dragovich et al., 1998, Dragovich et al., 2000). For the purposes of this study, however, I classify the Mt. Josephine semi-schist and the Darrington phyllite as separate rock units, albeit units that may be related and often similar in composition, structure, and mineralogy. A single K-Ar whole rock analysis for the Mt. Josephine semi-schist yielded a 113 ± 3 Ma metamorphic age (Misch, 1963; Misch, 1964; Tabor et al., 2003) but no prior protolith ages exist.

2.2.2 Darrington phyllite

The Darrington phyllite (Vance, 1957; Misch, 1966) is also one of the regional blueschist facies units of the Easton metamorphic suite. This unit mainly consists of graphitic

metasedimentary phyllite (described and mapped as the Silver phyllite in some locales by Tabor et al., 2002) or a siliceous argillite, with lesser metachert, Fe-Mn rocks, and psammite (Misch, 1996; Brown et al., 1982). The mineralogy of the phyllite consists of quartz, white mica, albite, graphite, pyrite, epidote, chlorite, with lesser amounts of oxides, lawsonite, spessartine garnet, and titanite. Dark gray to silver in color, the Darrington phyllite is a fine-grained unit that predominantly has a higher mica content than that of the Mt. Josephine unit. In some instances, at the contact between the Shuksan and the Darrington, Fe-Mn rich transitional rocks occur but are only a few meters in width (Haugerud et al., 1981, Dungan et al., 1983, Cordova et al., 2019). Recent white mica $^{39}Ar/^{40}Ar$ ages for the Darrington phyllite yielded metamorphic ages from 148 Ma to 142 Ma (Cordova et. al., 2019).

2.2.3 Shuksan greenschist

The Shuksan greenschist/blueschist unit (typically referred to as the Shuksan greenschist) is locally abundant throughout parts of western Washington state and makes up one of the main units of the Easton metamorphic suite (Fig 1). The Shuksan is composed of metabasaltic and metatuffaceous units of MORB affinity (Street-Martin, 1981; Dungan et al., 1983) and consists of finely interlayered greenschist and blueschist and local pillow basalts (Brown et al., 1982; Haugerud et al., 1981; Brown, 1986). The mineralogy typically consists of white mica, albite, epidote, actinolite and/or glaucophane with lesser amounts of garnet, stilpnomelane, titanite, pyrite, and calcite. Both the blueschist and the greenschist members of the Shuksan have the same mineralogy, except the blueschist rocks have sodic, not calcic amphiboles (Brown et al., 1982). The differences between the interlayered blueschist and greenschist appear to be from slight differences in protolith composition and Fe valence, rather than differences in metamorphic grade

(Haugerud et al., 1981; Dungan et al., 1983). White mica $^{39}Ar/^{40}Ar$ metamorphic ages from the Shuksan greenschist/blueschist unit range from approximately 140 to 136 Ma (Cordova et. al., 2019).

2.3 Previous U-Pb Zircon Constraints on Protolith Ages in the Easton metamorphic suite

Despite the well-documented metamorphic ages for various units in the Easton metamorphic suite, little information about protolith age and maximum depositional age of the regional blueschist units exist. Only four U-Pb zircon ages have been published regarding the Easton prior to this study (Fig. 1). Brown and Gehrels (2007) obtained a detrital U-Pb zircon age from the Mt. Josephine semi-schist (metagraywacke) in the Mount Josephine area of the Easton complex, with a 155 Ma peak (no maximum depositional age was calculated for that sample, only the peak age was reported). Zircon ages from metaigneous rocks in the western portion of the Easton complex range from 163-164 Ma (Brown and Gehrels, 2007; Gallagher et al., 1988; Dragovich et al., 1998), but the structural setting of these igneous rocks is contested. Gallagher et al. (1988) included the metaigneous rocks within the Easton nappe, but Dragovich et al. (1998) considered them to be in the Haystack nappe (Fig. 1). This study did not resolve the setting of these igneous units and instead focuses on samples that are definitively within the Easton metamorphic suite.

2.4 Competing Early Subduction Accretion Models

Existing studies in the Easton metamorphic suite have led to competing interpretations for the correlation and timing of accretion of individual units within the lower-grade regional blueschists. Two end-member models explain how the Easton was accreted and subducted in the

Jurassic. Brown et al. (1982) recognized that the regional blueschists (Mt. Josephine semi-schist, Darrington phyllite and Shuksan greenschist) were accreted later than the higher-grade amphibolite and blueschist but interpreted the regional blueschist as a single unit with the Darrington phyllite originally in depositional contact on the Shuksan greenschist prior to subduction (Haugerud et al., 1981). This model predicts that unit boundaries between the Shuksan greenschist and Darrington phyllite are primary depositional contacts and the units have a shared structural history. Previous researchers (Misch, 1966; Haugerud et al., 1981) also suggested that the contacts within the regional blueschist units were depositional in nature, rather than tectonic. Misch (1966) proposed that the Shuksan greenschist was above the Darrington phyllite with a depositional contact, whereas Haugerud et al. (1981) suggested that the Darrington phyllite overlaid the Shuksan greenschist, and still suggested the contact between units were primary. Based on the MORB-like signature of the Shuksan greenschist, Dungan et al. (1983) argued that an oceanic origin of the Shuksan protolith was not compatible with the interpretation of Misch (1966) (e.g., Shuksan stratigraphically overlying the Darrington) and recognized the need to better understand the structural history of the units.

In contrast, Cordova et al. (2019) combined microstructural analysis and $^{40}Ar/^{39}Ar$ dating (Fig. 2C) to show that the Darrington phyllite preserves an older metamorphic history not recognized in the Shuksan greenschist and suggested the two units have different subduction-accretion histories. Cordova et al. (2019) recognized two metamorphic events in the Darrington phyllite: 1) a S_1^P event older than 148 Ma and 2) a S_2^P event as young as 142 Ma. In contrast, the Shuksan greenschist preserves a 141 Ma S_1^G event that overlaps with the youngest Darrington ages, as well as a later S_2^G event at 136 Ma. From these metamorphic age estimates, this contrasting

model posits that the Darrington was subducted and metamorphosed earlier than the Shuksan greenschist, and that the units are separated by a structural (tectonic) contact.

3. METHODS

This study presents a combination of field and petrographic observations and new zircon U-Pb geochronology to reconstruct the accretion history and provenance of the regional blueschist units of the Easton metamorphic suite in the Jurassic. The results from this work are compared to previous U-Pb zircon geochronology in comparable units in the Northwest Cascades Thrust System (NWCS) and $^{40}Ar/^{39}Ar$ geochronology in the Easton metamorphic suite.

3.1 Field, Structural, and Petrographic Methods

To understand the structural histories of units in the Easton metamorphic suite, I conducted structural analysis of outcrops north and south of the Skagit river (Figs. 3, 4). At each of the 31 sampling sites in the study area (Fig. 3), I described and measured rock type, primary and secondary structures, metamorphic grade, and structural information to see if the units had shared or different deformation histories. In the field, the lithology of each sample was determined by color, mineralogy, grain size, texture, and weathering of the rocks. Additionally, I gathered a total of 40 oriented samples for petrographic and geochronology analyses.

I utilized the combination of a traditional Brunton compass and an iPhone 10XR with the field application FieldMove Clino to record structural measurements such as orientation of foliations, folds, lineations, original bedding indicators, shear zones, and boudins. Both the Brunton and the iPhone were calibrated at each outcrop to ensure that both methods produced similar measurements within one to three degrees of one another for strike, dip, and lineation data.

Calibration of the iPhone with the Brunton compass was necessary because smartphone devices and traditional compass measurements should be used together to ensure the quality and integrity of the field measurements, as the internal operating systems within smartphone devices can be susceptible to magnetic signals (Allmendinger et al., 2017). Once the calibration was completed, I took several measurements with the iPhone for greater efficiency and a higher number of measurements per outcrop. I then plotted the structural measurement data using Python and Stereonet (Version 10.0) to create stereographic representations of the orientation of foliation, folds, axial planes, and hinge lines.

Due to the general fine-grained nature of the low temperature blueschist samples in the Easton, petrographic analysis was necessary to determine the mineralogy and observe microstructures not visible in outcrops. I analyzed each individual thin section first for mineralogy, texture, and shape of minerals. Microstructures such as inclusion trails, relict and transposing fabrics, deformation intensity, and microlithon spacing were noted for each sample to infer deformation intensity and kinematics of the units. Microstructural observations such as crenulation spacing and transposition of older fabrics by younger fabrics offered insights into strain intensity and sense of shear.

3.2 U-Pb Zircon Geochronology Methods

For this study, I gathered twelve potential detrital U-Pb zircon samples. Due to the fine-grained nature of the units, I collected approximately 50 pounds of fresh, unweathered rock for each geochronology sample to try to ensure a sizable zircon yield during later-stage analysis. After the samples were crushed, the zircons were separated using a water table, Frantz Magnetic separator, and heavy liquid separation using diiodomethane to prepare for in-situ U-Pb analysis.

I analyzed six of the twelve samples for U-Pb detrital zircon and U-Pb igneous zircon geochronology to better understand the depositional ages of the Easton units (Fig. 3; Table 1). The five metasedimentary samples (four from the Mt. Josephine, one from the Darrington) were analyzed for detrital zircons (to yield a detrital, maximum depositional age) and one sample from the Shuksan greenschist unit was analyzed for igneous zircons (to yield an igneous crystallization or protolith age) (sample 192-30). I selected the samples based on two main criteria: 1) a relatively coarse grain size at the outcrop so that the zircon crystals would be larger and easier to analyze during U-Pb geochronology, and 2) overall location within the research area to ensure as representative a data set as possible.

Zircon U-Pb geochronology was performed at the University of Arizona LaserChron Center using a Thermo Element2 HR ICP-MS, coupled to Photon Machines Analyte G2 excimer lasers equipped with HelEX low-volume cells. Lab analyses and data reduction follow the methods outlined in Gehrels et al. (2008) and Gehrels and Pecha (2014), using spot sizes ranging from ~25 to 35 um and targeting cores of the detrital zircons and cores and rims for the igneous zircons (see supplemental tables). I outline the detailed zircon analysis techniques in Section 4.2 (*Detrital Zircon U-Pb Geochronology Results*) and I offer the context on how I use the maximum depositional age, accretion age, and protolith age in Section 5 (*Discussion*).

4. RESULTS

4.1 Lithologic Units, Mineralogy, and Structural Fabrics

For this study, I followed the naming convention outlined by Cordova et al. (2019) to identify fabrics and folds within the Easton units. Foliations are represented by the capital letter S and folds are represented by the capital letter F, followed by a number to indicate the generation

of the event in subscript, and another letter to indicate the rock unit in superscript (P = Darrington phyllite, J = Mt. Josephine semi-schist, G = Shuksan greenschist/blueschist). For example, S_1^J represents the first generation of foliation in the Mt. Josephine semi-schist, and F_2^P represents the second generation of folding in the Darrington phyllite.

4.1.1 Mt. Josephine semi-schist

The Mt. Josephine semi-schist usually occurs as a tan to gray, coarse-grained semi-schistose metagraywacke that in some locales does have a schist-like appearance with distinctive layers at both the outcrop and micro-scales (Figs. 5A and 6A-C). The unit varies from medium to coarse-grained, with weathering producing a rough sandpaper-like texture not seen in the Darrington phyllite (Fig. 5B). Locally, the Mt. Josephine semi-schist can have highly graphitic layers (Figs. 5C and 6A), but even those are often coarser grained when compared to the Darrington phyllite. Metachert can occur as clasts or thin layers within the semi-schist (Fig. 5B) and is more abundant in the westernmost outcrops of the semi-schist in the Blanchard Mountain area. The semi-schist is more common in the west (Mt. Blanchard study area) and at the type locality, the Mt. Josephine study area (Fig. 3, Table 1).

The Mt. Josephine semi-schist has two main fabrics, S_1^J and S_2^J, however, rare relict bedding (S_0^J) exists defined by grain size and composition changes (Fig. 5B, 6A). Quartz veins up to a few cm thick are also parallel to S_1^J (Fig. 5A, 6C). The S_1^J fabric is well-developed and defined by varying thicknesses of quartz-rich zones separated by mica-rich areas (Fig. 7A-B). The S_1^J fabric is the dominant fabric and anastomoses around larger grains of quartz and chert lithics that have been deformed and sheared (Fig. 8A-B). The second fabric (S_2^J) is poorly developed and defined by the crenulation cleavage in the semi-schist (Figs. 5A, 6D). Flattening strain and

dissolution indicators in the cleavage are present in both fabrics (Figs. 7B, 7D, 8B). In addition to quartz and white mica, graphite, chlorite, actinolite, epidote, stilpnomelane, pyrite, titanite, and oxides are also present mostly in the S_1^J fabric (Fig. 7A-D). Sample 192-27 from Mt. Josephine (Figs. 7C, 8C) is highly graphitic and has complex textures that could reflect either primary sedimentary structures or later deformation.

The Mt. Josephine semi-schist has two generations of folds, F_1^J and F_2^J. The rare F_1^J folds are isoclinal, the axial planes form the S_1^J, transpose bedding, and occur on the cm-scale, ranging from 25 to 40 cm in length (Figs. 5B, 6A). The second generation of folds (F_2^J) deform the S_1^J foliation and vary in scale from cm to meters and have symmetric parasitic folds in the hinges (Figs. 5A, 5D, 6B-C). The S_2^J fabric is axial planar to the F_2^J folds but is variably developed. The F_2^J folds are cylindrical, gently ESE plunging, upright to steeply inclined, NNE vergent, subangular, similar, close to tight, and harmonic (Figs. 5A, 5D, 6B, 10). Boudinaged and folded quartz veins are also common in the Mt. Josephine unit, especially near the hinges of the F_2^J folds (Figs. 5A, 6C).

4.1.2 Darrington phyllite

The Darrington phyllite generally occurs as a fine-grained graphitic phyllite with local interbeds of silt and fine sands, and prominent quartz veins (Figs. 5E, 6D-E). In rare cases, original bedding indicators (S_0^P) reflect differences in grain size within the phyllite (Figs. 5E and 6D). However, the original bedding layers are often overprinted by a foliation that is more prominent in the outcrop and identifying right way-up indicators is difficult due to the structural complexity of the units.

The Darrington phyllite unit has two main foliations, S_1^P and S_2^P, with S_2^P being the prominent foliation observed within the unit. The first fabric (S_1^P) is identifiable in thin section but often overprinted by the S_2^P fabric (Figs. 7E, 8D). The S_1^P foliation is locally preserved in albite porphyroblasts and in crenulation hinges (Fig. 8E-F), especially in the Iron Mountain study area. The axial planar S_2^P fabric overprints the S_1^P with varying intensity (Fig. 8D, G). Locally bedding layers are preserved (S_0^P), defined by finer and slightly coarser grains and graphite content (Fig. 8H). In most of the samples, there is evidence of undulose extinction of quartz and subgrain rotation (Fig. 8I). Like the Mt. Josephine semi-schist, the Darrington phyllite experienced pressure solution and volume loss during metamorphism and deformation.

The Darrington phyllite is dominantly folded by F_2^P folds that fold the S_1^P foliation on a scale ranging from mm to meters (Fig. 4). The F_2^P folds are cylindrical, gently NW plunging, steeply inclined, subangular, similar, tight to isoclinal, and harmonic (Figs. 6D-E, 10). The S_2^P fabric is axial planar to the F_2^P folds (Fig. 6D).

4.1.3 Observed differences between the Mt. Josephine semi-schist and Darrington phyllite

The Mt. Josephine semi-schist is a coarse- to medium-grained metagraywacke locally interlayered with phyllite that previous workers have presumed to be equivalent to the Darrington phyllite. This led to the interpretation that the two units are related and/or interlayered. For this work, I classify the two units separately from one another based on outcrop features, structure, grain size, and geochronological evidence (as discussed in Section 4.2 and Section 5.1).

When contrasting the Mt. Josephine semi-schist and the Darrington phyllite at any scale, the differences between the two units are subtle, but important. While the mineralogy of the units is similar, the Mt Josephine unit is coarser (Fig. 7A-D) and less micaceous. The degree of strain

in the Mt. Josephine appears to be less than the Darrington phyllite (Fig. 8). The semi-schist often has meta-chert clasts or layers that the Darrington does not have and lacks the folding typical of the phyllite (i.e. the F_2^J folds are not as common at the microscale and the semi-schist often is not as tightly folded as the Darrington). The variations in grain size seems to have resulted in a difference in fold style/tightness. Thus, separating these two units based on just the structural history or fold style might be problematic, and likely requires further analysis.

In direct contrast to the Darrington phyllite, the Mt. Josephine semi-schist lacks the presence of large albite porphyroblasts with an older fabric defined by graphite inclusions preserved in the core (Fig. 8E-F). Darrington phyllite from the Iron Mountain study area contains large, texturally zoned albites that the other exposures of the Darrington in the western study areas lack, and this albite porphyroblast-bearing assemblage is what Tabor et al. (2002) refer to as the Silver phyllite. The albite porphyroblasts preserve the S_1^P fabric at a low angle to the later, more pervasive S_2^P fabric. The white mica in the matrix also shows the two different generations of the fabrics and the S_1^P fabric in the Darrington is only preserved in the microlithons between the more dominant S_2^P fabric (Fig. 8E-F). The presence of the albites in the Darrington phyllite suggest that there could be an older metamorphic history that is not recorded in the Mt. Josephine unit, offering further evidence of why these units should not continue to be considered equivalent.

4.1.4 Shuksan greenschist

In the Iron Mountain study area (Figs. 3, 4B), the Shuksan greenschist dominantly occurs as an interlayered greenschist/blueschist unit with the compositional difference between the two varieties observed at the outcrop and thin-section scale (Fig. 9A). The Shuksan greenschist is not

exposed in the Blanchard Mountain area and the Mt. Josephine area (Fig. 3) and is mostly present in the Iron Mountain study area.

The Shuksan greenschist/blueschist has two fabrics S_1^G and S_2^G observed in outcrop and thin section. The first fabric of the Shuksan (S_1^G) is a pervasive foliation of aligned metamorphic mica and amphibole as well as compositional layering (Figs. 5F, 7F, 9B). The small-scale interlayering of the greenschist and blueschist layers are defined by a change from actinolite to glaucophane (Fig. 9A). The S_1^G foliation is folded by the dominant second-generation folds (F_2^G, described below) (Figs. 5F, 6F-H) that commonly have an axial planar foliation (S_2^G) (Figs. 6G, 7F) defined by aligned actinolite/glaucophane, muscovite, chlorite, and epidote with minor oxides (Fig. 9A-B). The development of the S_2^G foliation is variable but regularly observed in F_2^G fold hinges (Fig. 6G). In the Iron Mountain location, small shear zones (~1 to 2 m wide) occur in the Shuksan greenschist. These zones are characterized by finely crystalline mylonites with garnet porphyroblasts, epidote porphyroclasts, and zones of both blue and green amphiboles (Fig. 9C).

The Shuksan S_1^G is pervasively folded by F_2^G folds on a scale that ranges from cm to meters (Fig. 4B). The F_2^G folds are cylindrical, gently SE plunging, steeply inclined, NE vergent, subrounded, similar, tight to isoclinal, and harmonic (Figs. 5F, 6F-H, 10).

4.2 Zircon U-Pb geochronology results

Of the six samples collected for geochronology, only four samples (192-15, 192-21, 192-27, and 192-30) had a sizable enough zircon yield to interpret. The two low zircon yield samples (192-10 and 192-20) are still included below for comparison. The results are presented as Wetherell-concordia plots (Fig. 11), kernel density estimate (KDE) plots (Fig. 12), cumulative age

distributions (CAD) plots (Figs. 13, 14), radial plots (Fig. 13), YC2σ(3+) age diagrams (Fig.15), weighted mean plots (Figs. 16-17), and a TuffZirc plot (Fig. 17).

For analysis of the U-Pb zircon results, I used both Isoplot-R and Python scripts (detritalpy version 1.3.26) to create the plots presented in this study, following the methods by Vermeesch (2018) and Sharman et al. (2018), respectively. I considered grains that were concordant within a 2σ uncertainty for the age calculations. I calculated maximum depositional ages using the YSC2σ(3+) age as a conservative estimate, which sorts all analyses by their U-Pb age plus 2σ uncertainty, and identifies the youngest cluster of 3 or more analyses with overlapping 2σ error (Dickinson and Gehrels, 2009; Sharman et al., 2018). For the two detrital analyses that had a low zircon yield, I used a combination of the YSC2σ(3+) age and weighted mean calculations to estimate the probable maximum depositional age for those units to compare with the higher N analyses. For the Shuksan greenschist analysis, I used a combination of a weighted mean age and the TuffZirc age to infer protolith age. The TuffZirc model attempts to present the best age from a set of analyses by identifying the tightest cluster of ages and calculates the weighted mean from that cluster of ages. This method also assumes that some of the younger ages are likely affected by Pb loss and takes that into account (Gehrels et al., 2008; Gehrels and Pecha, 2014).

4.2.1 Mt Josephine semi-schist

Samples 192-10, 192-15, 192-21, and 192-27 (Fig. 5A-D) were collected for their coarse grain size and location within the study areas to ensure a sizable zircon yield for geochronology analysis (Fig. 3, Table 2).

Sample 192-15 (semi-schist of Mt. Josephine from Blanchard Mountain) was collected towards the western extent of the Easton metamorphic suite and was one of the coarsest-grained

samples taken for detrital zircon analysis (see Fig. 3, Table 1 for location). This sample had a total zircon yield of 239 grains (N = 239) (Fig. 11A; gray curve on Fig. 12A-B). Of those 239 grains analyzed, 227 were concordant (n = 227) (black curve on Fig. 12A-B). The kernel density estimate of this sample has a prominent peak at 153 Ma, with small, scattered peaks at ~200 Ma and ~229 Ma (Fig. 12A-B). The sample has populations of concordant grains around 1.0 Ga and 1.5 Ga. The cumulative age distributions (CAD) plots show ~80% of grains ≤153 Ma (the peak age, red line on Figs. 13A, 14). The radial plot shows a similar prominent peak with ~89% of analyses falling near 158.2 Ma, and a smaller percentage pointing toward an older peak at 1.1 Ga (Fig. 13A). The YC2σ(3+) age is 144.1 ± 1.16 Ma (Fig. 15A). This age is interpreted to represent the maximum depositional age of Mt. Josephine sample 192-15.

Sample 192-21 (Mt. Josephine semi-schist east of Blanchard and Colony Mountain) was collected in the western extent of the Easton metamorphic suite but is located east of sample 192-15 (Fig. 3, Table 1). This sample had a total zircon yield of 282 grains (N = 282) (Fig. 11B, gray curve on Fig. 12C-D). Of the 282 grains analyzed, 266 were concordant (n = 266) (black curve on Fig. 12C-D). When all grains are plotted with no discordance filter, the max peak age of the kernel density estimate is 147 Ma. Additional smaller, scattered peaks on the KDE occur around 191 - 196 Ma, 400 Ma, and older populations at 1.0 Ga, 1.4 Ga, and 1.75 Ga (Fig. 12C-D). The CAD plots show ~75% of grains younger than the max peak age of 147 Ma (red line on Fig. 13B, Fig. 14). The radial plot shows a prominent peak with ~74% of analyses plotting near the 151.6 Ma zone (Fig. 13B). The YC2σ(3+) age is 121.3 ± 2.32 Ma (Fig. 15B) and is interpreted to represent the maximum depositional age of Mt. Josephine sample 192-21.

Sample 192-27 (semi-schist of Mt. Josephine near Mt. Josephine) was collected in the eastern extent of the study area, north of both the Skagit River and the Iron Mountain study area

(see Fig. 3, Table 1 for location). This sample had a total zircon yield of 243 grains (N = 243) (Fig. 11C, gray curve on Fig. 12E-F). Of the 243 grains analyzed, 150 were concordant (n = 150) (black curve on Fig. 12E-F). When all grains are included with no discordance filter, the youngest peaks on the KDE plot have a bimodal distribution with a 123 Ma peak and a 170 Ma peak (Fig 12E-F, Fig. 14). Slightly older grains occur between ~200 to 280 Ma, but there are lots of scattered Precambrian grains between ~1.0 Ga and 2.7 Ga (Fig. 11). The CAD plots show two subsets of distributions: 20% of grains are younger than the peak age of 123 Ma (1st red line on Fig. 13C, Fig. 14) and the second shows 50-55% of grains are younger than the peak age of 170 Ma (2nd red line on Fig. 13C, Fig. 14). The radial plot shows a prominent peak with ~56% of analyses around 160 Ma and ~20% smaller grouping around the 1.9 Ga (Fig 13C). The YC2σ(3+) age is 122.9 ± 0.84 Ma (Fig. 15C) and is interpreted to represent the maximum depositional age of Mt. Josephine sample 192-27.

Sample 192-10, a Mt. Josephine semi-schist from Blanchard Mountain, had a low zircon yield, like Darrington phyllite sample 192-20 (Fig. 3, Table 2). Because of the low N for this Mt. Josephine sample (N = 8) the kernel density estimate was not plotted. The YC2σ(3+) age is 157.2 ± 3.82 Ma and the weighted mean of the youngest population of concordant grains was 154 ± 11 Ma (Fig. 16A). The YC2σ(3+) age represents the best estimate for the maximum depositional age of sample 192-10 within the Mt. Josephine semi-schist.

4.2.2 Darrington phyllite

Darrington phyllite sample 192-20 (from Lake Samish) (Fig. 5E) was collected from the westernmost extent of the Easton Suite in the Blanchard Mountain study area for the relatively coarse grain size (Fig. 3, Table 2). Because of the low N for this sample (N = 14) the kernel density

estimate was not plotted. The YC2σ(3+) age is 151.9 ± 2.54 Ma and the weighted mean of the youngest population of concordant grains is 152 Ma ± 1.33 Ma for sample 192-20 (Fig. 16B). The YC2σ(3+) age represents the best estimate for the maximum depositional age of the Darrington phyllite sample 192-20.

4.2.3 Shuksan greenschist

Sample 192-30 is a Shuksan greenschist/metatuff from Iron Mountain and was the only geochronology sample of the six analyzed that was collected in the Shuksan greenschist unit (see Fig. 3, Table 1 for location). The Shuksan greenschist Sample 192-30 (Fig. 5F) was sampled to determine the igneous crystallization (protolith) age. (Fig. 3, Table 2).

This sample had a total zircon yield of 42 grains (N = 42) (Fig. 11D, gray curve on Fig. 12G-H). Of the 42 grains analyzed, 37 grains were concordant (n = 37) (black curve on Fig. 12G-H). With no discordance filter applied, the largest peak on the KDE plot occurs at 159 Ma (Fig. 12G-H). Scattered concordant grains occur approximately near 600 Ma and 1.0-1.6 Ga (Fig. 11D, 12G-H). The CAD plot shows ~40% of grains are younger than the max peak age of 159 Ma (red line on Fig. 13D). The radial plot shows a prominent peak with ~43% of analyses at 166.8 Ma (Fig. 13D). The TuffZirc age of the coherent group of 6 grains is ~166 Ma with a confidence of 96.9% and the weighted mean is also 166.31 ± 1.37 Ma (Fig. 17). The weighted mean age likely represents the protolith age of Sample 192-30. The younger ages around 116 ± 9 Ma and ~50 Ma (Fig. 13D) are high in U (see supplemental table) and are likely affected by Pb loss.

5. DISCUSSION

The primary purpose of this study was to better understand relationships between regional blueschist facies units of the Easton metamorphic suite using structural analysis and U-Pb zircon geochronology. In what follows, I use the data above to: 1) constrain the protolith and maximum depositional ages of the units; 2) evaluate the correlations and extent of metasedimentary units; and 3) estimate the duration of the Easton accretion in the Northwest Cascades Thrust System (NWCS). Previous studies working in the Easton nappe have provided metamorphic white mica and $^{40}Ar/^{39}Ar$ ages and metamorphic temperature estimates, but limited U-Pb zircon age data. Additionally, I discuss the different depositional environments of the regional blueschist units, their possible sources, and the tectonic implications of the maximum depositional ages (MDAs) within the Easton and adjacent units for subduction accretion along the North American margin.

In order to use and compare the new U-Pb zircon ages presented in this study, I offer the following context on how I interpret the different age estimates. The maximum depositional age (MDA) is a minimum estimate of when the unit could have been deposited and places an upper age estimate on the sample since it must predate the time of true deposition (e.g. an MDA of ~144 Ma means that it is likely it was deposited at most 144 Ma or a time younger than that age). Meaningful maximum depositional ages have an N > 100 grains, but ages with N > 300 are best (Coutts et al., 2019). Previous research has indicated that sediments at accretionary margins often get subducted soon after deposition (Cawood et al., 2012; Dumitru et al., 2018), indicating that maximum depositional age estimates can approximate accretion ages (Apen et al., 2021, Dumitru et al., 2015; 2010; Snow et al., 2010). The protolith age in this study is used as an estimate for when the Shuksan unit was first erupted or crystallized because the protolith for the unit is interpreted to be volcanic. By estimating the maximum depositional ages (and by inference the

depositional age and accretionary age) of the metasediments in tandem with the protolith age of the Shuksan, I attempt to compare the provenance history of the blueschist units within the Easton.

5.1 Age Relationships of the Mt. Josephine, Darrington, and Shuksan units

The maximum depositional ages of the metasedimentary units sampled in the Easton metamorphic suite support the hypotheses that the Darrington phyllite and Mt. Josephine semi-schist are not the same unit, have different depositional histories, that the Mt. Josephine semi-schist may have two sub-units, and that the Darrington phyllite is likely older than the Mt. Josephine semi-schist. This work obtained five new detrital ages, with four of the five detrital samples coming from the Mt. Josephine semi-schist, and the remaining sample coming from the Darrington phyllite (Table 1). Two of the five samples had a low zircon yield (samples 192-10 of the Mt. Josephine and 192-20 of the Darrington, black stars on Fig. 3). For the three Mt. Josephine samples that had a high return of zircon grains (yellow stars on Fig. 3), Sample 192-15 yielded a maximum depositional age of 144.1 ± 1.16 Ma, Sample 192-21 yielded a maximum depositional age of 121.3 ± 2.32 Ma, and Sample 192-27 yielded a maximum depositional age of 122.9 ± 0.84 Ma (Fig. 15). From the data, there are two probable sets of maximum depositional ages within the meta-sedimentary Mt. Josephine unit: the first ~144 Ma and the second ~122 Ma. The sample from the Mt. Josephine study area (192-27) was the only semi-schist sample to have a distinctly bimodal distribution for its KDE plots, with the two main peak ages of 170 Ma and 123 Ma, and a third, smaller intermediate peak around 146 Ma (Figs. 12F, 14). This is notable because it records the two MDAs established for the other semi-schist samples (~122 Ma and ~144 Ma) but shows an almost complete continuum of ages from 170 to 122 Ma.

The greater than 20 m.y. difference in maximum depositional ages between samples of the Mt. Josephine semi-schist could be attributed to episodic accretion, different depositional environments, and/or sediment source during deposition. For the two samples (192-21 and 192-27) with the MDA at ~122 Ma, the samples also contain grains near 144 Ma, indicating the source area could be somewhat like the sample with the ~144 Ma MDA, but just with fewer grains of that age included in the sample. Alternatively, there could be different aged units in what is collectively considered the Mt. Josephine semi-schist. The ~144 Ma MDA sample (192-15) did not have any grains near 120 Ma like the samples in the younger portion of the Mt. Josephine do. The two ~122 Ma MDA samples from the Mt. Josephine have a subset of grains younger than the those in the older MDA sample, which suggests that the sample with the ~144 Ma MDA is truly different than the two samples with the calculated MDA of ~122 Ma (i.e. Sample 192-21 had 10 grains near the MDA and Sample 192-27 had 19 grains near the MDA). Upon comparing all three high-N Mt. Josephine samples, the samples all have different detrital zircon signatures, suggesting that the Mt. Josephine is internally complex. Whether the Mt. Josephine semi-schist is truly a different unit than the Darrington phyllite is a critical question to consider when evaluating the relationship between the regional blueschist units.

Though the single Darrington phyllite geochronology sample had a low zircon yield, the 151.9 ± 2.54 Ma YC2σ(3+) age represents the best estimate for the maximum depositional age of the Darrington phyllite and lends insight into the differences between the Darrington phyllite and Mt. Josephine semi-schist units (Fig. 18). Upon comparing the MDAs of the Mt. Josephine samples and the Darrington sample, the results posit that all high-N Mt. Josephine MDAs are younger than the 152 Ma MDA age of the Darrington phyllite (Fig. 16B). Because of the low number of zircons from this Darrington geochronology sample, the 152 Ma MDA age presented

in this study carries a higher degree of uncertainty than the Mt. Josephine semi-schist ages. The weighted mean age of the Darrington sample is 152 ± 1.33 Ma, and further confirms the similar YC2σ(3+) MDA age. The next closest age to the Darrington MDA of ~152 Ma is the other low N sample from the Mt. Josephine (Fig. 16A) that yielded a 157.2 ± 3.82 Ma YC2σ(3+) MDA age. Both the YC2σ(3+) MDA ages and the weighted mean ages of samples 192-10 (Mt. Josephine) and 192-20 (Darrington) do have some overlap at their 2σ uncertainties. These two westernmost geochronology samples are closest to one another spatially (Figs. 3, 4A) but are low N samples, so it is possible that the youngest grains might not have been captured in the analysis of each sample. The ~152 Ma MDA of the Darrington also is consistent with the metamorphic ages presented by Cordova et al. (2019) which places metamorphism of the unit from ~148 - 142 Ma. Thus, the time between the estimated maximum deposition and metamorphism in the Darrington is relatively quick at only ~ 4 m.y.. Because of the uncertainty of the ~152 Ma age from the Darrington phyllite, additional detrital zircon geochronology in the Darrington phyllite is needed to confirm the results presented here.

Based on the lithological, structural, and geochronological factors presented in this study, I argue that the Darrington phyllite and the Mt. Josephine semi-schist are not equivalent units. The two units have varied grain sizes and some lithologic differences, with the Darrington occurring as a finer-grained phyllite and the Mt. Josephine occurring as a coarser-grained metagraywacke. While both the Mt. Josephine and Darrington have fold sets that are gently plunging and steeply inclined, their orientations are slightly different (Fig. 10) and the Darrington phyllite folds are tighter and had shorter wavelengths when compared to the semi-schist. While minor, this could reflect a difference in competency of the different sediments during metamorphism and deformation. The difference in structural history could also be the result of varying strain gradients

combined with the behavior of the rocks as they deformed depending on how thick the clastic versus pelitic layers are. On the microscale, the semi-schist commonly has meta-chert clasts and layers that the Darrington lacks (Fig. 5B). However, the exposures of Darrington mineralogy in the east (Iron Mountain study area) notably have large, zoned albite porphyroblasts that preserve an earlier S_1^P fabric in the cores (Fig. 8E-F) and that are absent in the Mt Josephine semi-schist. This is an important distinction because it appears that the Mt. Josephine does not have the earlier fabric that is recorded in the S_1^P of the Darrington phyllite. Since the main fabric in the Darrington is S_2^P, whereas the main fabric for the Mt. Josephine is S_1^J, this difference could be the result of rheology but also could be due to a different number of metamorphic events. It is possible there is an older metamorphic component to the Darrington phyllite, perhaps the one with the albite porphyroblasts, but without more geochronology ages it is difficult to know for certain.

These small, but important, differences between the Darrington phyllite and Mt. Josephine semi-schist further reinforce that they are not the same unit, nor should they continue to be classified as such (Fig. 18). If we use maximum depositional ages to differentiate the Darrington and Mt. Josephine, then the grain size factors that have historically been the dominant way used to separate them may not be the most accurate method to distinguish the two regional units. Splitting the Darrington and Mt. Josephine units in the field seems to be the prevailing challenge, which is also affected by the scale at which the units might be structurally interlayered or faulted. Thus, there is a possibility that some of what we have classified as the Darrington phyllite could be grouped into the Mt. Josephine semi-schist, and perhaps the Darrington phyllite could be split into more units than it is currently. It is clear there is a need for future detrital zircon geochronology and detailed mapping within the Darrington phyllite and Mt. Josephine semi-schist units to resolve these lingering problems.

The maximum depositional ages of the Darrington and Mt. Josephine units compared to the protolith age from the Shuksan greenschist supports models that argue the Darrington phyllite is younger and "depositional" on the Shuksan greenschist. Previous researchers proposed that the age of the oceanic protolith of the Easton metamorphic suite was Late Jurassic (Armstrong, 1980; Brown et al., 1982). A probable Mid-Jurassic protolith age for the Easton was indicated by a U-Pb zircon age of 163 Ma from a diorite on Bowman Mountain (Fig. 1), that was interpreted by Gallagher et al. (1988) to form the basement and sub-arc plumbing to the volcanic clast-bearing Mt. Josephine semi-schist (Dragovich et al., 1998; Brown, 1986). The mid-Jurassic weighted mean age of 166.31 ± 1.37 Ma (Fig. 17) from the Shuksan sample in this study supports the models which argue for the Darrington sediment being deposited upon the older, volcanic Shuksan unit on the seafloor (Fig. 18) (Haugerud et al., 1981; Brown et al., 1982). The spread of Precambrian grains from the Shuksan sample points towards a more complex source for the protolith (Fig. 11). There seems to be a certain degree of inheritance for this sample as the data do not necessarily reflect a clear igneous zircon signature, but perhaps could reflect more of a clastic rock with reworked zircons. Yet, previous geochemical analyses of the Shuksan have argued that these rocks have a standard tholeiitic basalt chemistry and mid-ocean ridge basalt affinity (Street-Martin, 1981; Dungan et al., 1983). Perhaps an explanation for the inheritance of older grains in the Shuksan sample has to do with some sedimentary component included within the tuffaceous material, and could point towards the portions of the Shuksan protolith having an eruption nearby the continental margin. Additional protolith ages of the Shuksan could help confirm or deny this hypothesis.

The interpretation that the Darrington phyllite was deposited on the Shuksan greenschist contrasts with the most recent metamorphic ages and model proposed by Cordova et al. (2019).

The youngest fabric in the Darrington phyllite (S_2^P) was dated at 148-142 Ma (Fig. 2) and overlaps with the age of the oldest fabric within the Shuksan greenschist (S_1^G), dated at 140 Ma. Thus, the Darrington phyllite appears to record an older metamorphic history and was accreted earlier than the Shuksan greenschist. The two Shuksan greenschist fabrics (S_1^G and S_2^G at ~140 and 136 Ma, respectively) were formed > 25 m.y. after the Shuksan protolith was created around 166 Ma, which is a much longer gap in time compared to the other regional blueschist units.

5.2 Correlations Within the Northwest Cascades System

I offer a comparison with three other units in the Northwest Cascades Thrust System to highlight that the new detrital zircon record I present in this work has nearby analogues, based on similar maximum depositional ages, similar structural position in the nappe sequence, and similar lithologies. Brown (2012) maps two separate nappes structurally below the Easton, the Lummi and the Constitution (Fig. 1), both of which are composed of siltstone, shale, and greywacke (Vance, 1975). Like the Easton, both the Lummi and Constitution Formations have oceanic and arc components and were affected by high-pressure/low-temperature metamorphism (Vance, 1975; Brandon et al., 1988; Burmester et al., 2000; Lamb, 2000). The Fidalgo Complex is made up of slightly metamorphosed igneous and sedimentary rocks typically included within an ophiolite sequence (Brown, 1977; Gusey, 1978). The sedimentary cover sequence of the Fidalgo Complex is in a higher structural position within the Haystack nappe and does not record high pressure/low-temperature metamorphism, but still offers another useful MDA comparison within the NWCS (Fig. 19).

Analyzing the data of Brown and Gehrels (2007) using the same methods as in the current study shows that the Constitution and Lummi Formations and Fidalgo Complex within the

Northwest Cascades System nappes have similar kernel density estimates, cumulative age distributions, and maximum depositional ages to the metasedimentary units of the Easton metamorphic suite (Fig. 20).The sedimentary rocks from the Constitution, Fidalgo, Lummi, and Easton metamorphic suite (Brown and Gehrels, 2007; this study) dominantly show unimodal detrital zircon populations between ~160-140 Ma (Fig. 20) with their associated YC2σ(3+) ages (maximum depositional ages) between ~145-130 Ma (Fig. 21). When comparing the units based on their ranked ages, the Mt. Josephine and Lummi Formation samples from Brown and Gehrels (2007) are the most similar with respect to their MDA range, from ~ 145 to 143 Ma (Fig. 20). The Mt. Josephine sample yielded a peak age of 154 Ma and an MDA of 145.6 ± 1.48 Ma (Figs. 20, 21), and the Lummi sample yielded a peak age of 148 Ma and an MDA of 143.5 ± 1.06 Ma. While the Mt. Josephine sample from Brown and Gehrels (2007) recorded the oldest MDA for the semi-schist unit at ~145 Ma, this age is nearly equivalent to the MDA for the older Mt. Josephine sample from this study (192-15), which yielded a 144.1 ± 1.16 Ma MDA and peak age of 152 Ma (Figs. 14-15). The next most similar units with respect to their MDAs are the Fidalgo and Constitution samples from Brown and Gehrels (2007). The Fidalgo sample yielded a peak age of 149 Ma and an MDA of 139.3 ± 1.42 Ma and the Constitution sample yielded a peak age of 150 Ma and an MDA of 130.7 ± 2.12 Ma (Figs. 20-21). The youngest maximum depositional ages from these four similar metasedimentary NWCS units were two Mt. Josephine semi-schist samples from thus study, 192-27 and 192-21, which yielded 122.9 ± 0.84 Ma and 121.3 ± 2.32 Ma, respectively (Figs. 14-15).

The Lummi Formation and the certain parts of the Mt. Josephine semi-schist in the Easton metamorphic suite could be correlative based on their structure, lithology, and maximum depositional ages. When compared to the Constitution Formation, the Lummi Formation has at

least two fabrics, has isoclinal folds, is coarser in grain size, and is separated by fault contacts (Lamb, 2000; Vance, 1975) much like the Mt. Josephine semi-schist. Previous researchers have noted the similarities between the Lummi Formation and the Easton (e.g. Brown, 2012) and these two units have been further likened to portions of the Klamath Mountains in California (Brown and Gehrels, 2007). The sedimentary cover sequence of the Fidalgo Complex is only younger than the Mt. Josephine and Lummi units by <5 m.y. and is older than the Constitution by nearly 9 m.y. (Figs. 20-21). However, the Constitution Formation's ~130 Ma MDA is more like the younger subset of the Mt. Josephine ages presented in this study at ~122 Ma. When viewed together, these depositional ages of other comparable units within the NWCS help confirm the new detrital record I present in this work.

5.3 Depositional Environments and Provenance of the Regional Blueschist Units of the EMS

Interpretations of the depositional environments of protoliths of the Easton metamorphic suite can be made by comparing the regional blueschist units from west to east. From the nature of the lithologic differences, the units have had related, but not identical, depositional environments. The western portion of the Easton metamorphic suite is dominated by metasedimentary rocks, with more of the Mt. Josephine semi-schist and less Darrington phyllite, but is mostly clastic in nature (i.e., mud, sand, and gravel protoliths). The eastern portion of the Easton in my study area is mostly composed of the metavolcanic rocks of MORB affinity, with smaller amounts of oceanic metasediments, as well as the metamorphic sole units near Iron Mountain. A near-arc setting was one of the first hypotheses for the western part of the Easton suite (Gallagher et al., 1988). As a large part of the western portion is the Mt. Josephine semi-schist, these areas likely could represent sedimentation near an island or continental arc (Dragovich

et al., 1998). The areas that are coarser-grained, not fully recrystallized probably were the proximal facies of a submarine turbidite, whereas the phyllite-rich areas (Darrington phyllite) probably were more distal facies of a submarine fan. The smaller amounts of chert and lesser volcanic detritus presumably contributed to the clastic material for the meta-sandstones in the Easton (Dragovich et al., 1998). Yet, when comparing the three coarse Mt. Josephine samples with a high-N, the variable peak distributions and differing MDA values perhaps suggest that using a field criteria like grain size and appearance to separate the Mt. Josephine and Darrington phyllite units alone is problematic.

An evaluation of clast lithologies within the metasedimentary units of the Easton helps refine the probable depositional environments of the Darrington and Mt. Josephine units. Listed by increasing order of abundance, the main lithology of clasts in the metasediments in the Mt. Blanchard study area as outlined by Gallagher et al. (1988) include: intermediate to felsic volcanic rock, monocrystalline quartz (metachert), quartz, plagioclase, gabbro/diorite, basalt/andesite, shale, epidote, and chromite. Some of the semi-schists were noted to be composed of almost entirely volcanic lithic fragments with extreme attenuation of up to 60 cm in length (Gallagher et al., 1988). These findings led Gallagher to the conclusion that the semi-schists contained detritus from meta-igneous rocks and "a virtual continuum of lithologies", further cementing the idea that these regional rocks likely accumulated in the same depositional basin, that the volcanic rocks were deposited with the sediments of the Darrington phyllite, and that the nearby mafic to intermediate plutonic rocks shed detritus into the basin (Gallagher et al., 1988). However, the term Mt. Josephine semi-schist was not in use while Gallagher was conducting his work and was only coined about a decade later by Dragovich et al. (1998).

Some researchers argue that it is relict chert clasts, not volcanic clasts, that comprise the major detrital clast component in the metasedimentary units, making their provenance more complicated. For the semi-schist and the phyllite, a mafic volcanic arc to quartzose provenance suggests a near-island or continental volcanic arc origin (Dragovich et al., 2000), since evidence for Easton near-arc deposition, rare tuffaceous greenschist layers in the semi-schist, and the presence of the volcanic clasts exists. A quartz-rich source of granitic erosion could also explain the relict quartz clasts (Roser and Korsch, 1986), meaning the Easton could be sourced by an arc and a continental basement (Dragovich et al., 1998; Dragovich et al., 2000). Yet, Dragovich noted that the volcanic relict clasts are an important aspect of the semi-schists but not the dominant component. Rather, the chert-rich source with minor elements of the volcanic arc detritus points towards a potential recycling of basin sediments during erosion of chert-rich basement rocks (Dragovich et al., 2000) from accreted terranes on the North American margin. Mineralogic observations also do not support the idea that the metasediments derived from the erosion of the greenstone only but were likely derived from a combination of uplifted sea-floor chert, quartzose basement rock, and highland volcanic rock (Brown, 1987; Dragovich et al., 1998; 2000). For the post-Gallagher classification of the western exposures of the Mt. Josephine, the semi-schist is different than the Darrington, which is one of the reasons why Dragovich separated the two while mapping, though it was more on a gradational scale (e.g. 20% Darrington, 80% Mt. Josephine). From the field observations of my study, when I observed clasts, I mainly found chert clasts, were the dominant clast type in the metasediments of the Mt. Josephine semi-schist in the Blanchard Mountain study area.

While the Easton metamorphic suite's possible depositional environments has remained the subject of debate for decades, two prevailing models exist for explaining the types of settings

the Easton was deposited into: 1) a back-arc model; or 2) subduction of a large ocean basin outboard of a continental margin. The back-arc model suggests that volcanic detritus in the western portion of the Easton is evidence of an arc to the west of the depositional basin with North America to the east (Gallagher et al., 1988; McDonald and Dragovich, 2015). This idea is further supported by the presence of meta-igneous rocks found in the westernmost extent of the Mt. Josephine semi-schist in the Blanchard Mountain study area. These gabbros, diorites, and metatuffs are all interpreted as arc-derived lithologies (Gallagher et al., 1988). The Darrington phyllite is also considered to be similar in composition to modern back-arc basin turbidites (McDonald and Dragovich, 2015). The highly graphitic component of the Darrington and parts of the Mt. Josephine semi-schist further lends credence to the hypothesis that the metasediments could have been deposited in a back-arc basin (Haugerud et al., 1981).

In contrast to the back-arc basin hypothesis, a large ocean basin is another likely depositional environment for the Easton based on the thermal history and duration of subduction metamorphism. By using typical rates of convergence at ~4cm/yr for 31 m.y. of subduction, Cordova et al. (2019) argued that a minimum of 1,200 km of ocean floor would have to be subducted to explain the duration of metamorphic and cooling ages within Easton metamorphic suite. That is not consistent with the typical widths of back arc basins, which are often on the smaller size range of at least 200 km. Based on the minimum duration of subduction coupled with the thermal history of the Easton, Cordova argued that a back arc basin was not as likely a depositional environment as a large ocean basin. However, if the back-arc closed via highly oblique subduction, the convergence would take a longer amount of time, and would not as strongly support the ocean basin model. Yet the presence of carbonaceous sediments within the Darrington and Mt. Josephine further corroborates that these metasedimentary units were probably

deposited in a basin without circulation from the open ocean (Gallagher et al., 2000; Haugerud et al., 1981). Therefore, the Easton was most likely deposited in an oceanic basin bordered to the west by an arc.

Though the Late Jurassic - Early Cretaceous zircons dominate the Easton samples presented in this work, there is a small signature of pre-Mesozoic and Precambrian grains. The pre-Mesozoic grains point towards a central North American source that has been recognized in nearby areas, like the Great Valley forearc basin between the Franciscan Complex and the Sierra Nevada magmatic arc (Orme and Surpless, 2019). Similarly, the small signature and inclusion of the Precambrian detrital zircons in the eastern Shuksan first noted by Tabor et al. (1988) and documented within this study hints at the proximity of the North American Craton or sediments derived from it to the east.

Precambrian zircons found in Shuksan-related rocks within the central Washington Cascades have long been argued to reflect a North American craton detrital component (Tabor et al., 1988). The eastern most sample in the Mt. Josephine semi-schist (192-27) had significantly more Precambrian grains than the other more westward Mt. Josephine samples from the Mt. Blanchard study area. The older zircon grains in the Easton samples from this study have relatively distinct populations around 1.0 Ga, 1.4 Ga, and 1.6 Ga (Figs. 11-12). While rocks in the Franciscan Complex also record the ~1.4 Ga zircon cluster, arguments based on the Franciscan and the Easton having similar tectonic histories or similar sources are potentially warranted, even though recent geochronologic data (Cordova et al., 2019; this study) has proven they are not necessarily a direct comparison for one another. Researchers working on rocks in a similar position within the Franciscan Complex do not believe these rocks were deposited into a back-arc basin, rather, they record long-lived E-dipping subduction (Saleeby, 1996; Shervais, 2001). Other researchers have

postulated that some of this older zircon material (>1.0 Ga) could be sourced from anorogenic granites, or the even older Belt supergroup based on their kernel density estimate peaks (Sauer et al., 2017).

One of the most important findings of this study has been the documentation of near continuous Late Jurassic - Early Cretaceous zircons from ~170 - 122 Ma. Interestingly, most zircons in the Easton samples fall in the ~155 to ~120 Ma age range, which spans most of the magmatic lull in the Sierras (Fig. 22). This magmatic lull is an important feature in the tectonic development of the Cordillera and has been well-constrained and well-documented in the Sierra Nevada batholith (e.g., Armstrong and Ward, 1993; DeGraaff-Surpless et al., 2002). The nearby Wrangellia terrane and its associated back arc basin (Kahiltna) lack zircons ~144 and 125 Ma (Kalbas et al., 2007; Hampton et al., 2010), as do many other possible sources. Thus, this magmatic lull necessitates that sources for these Late-Jurassic to Early Cretaceous grains recorded in the Easton regional blueschists were somewhat limited.

The Klamath and Blue Mountains of Oregon and California (Brandon et al., 1988) could be correlative to the rocks of the Easton and the other nappes of the NWCS (Brown, 2012) as rocks from the Sierra Nevada-Klamath regions have long been thought to be a potential provenance for the Easton zircons (Brown and Gehrels, 2007; Brown, 2012). Maximum depositional ages from the blueschists of the South Fork Mountain Schist in the Franciscan Complex (shown on Fig. 22) show similar ages to the older subset of the Mt. Josephine MDA estimate from this study (Dumitru et al., 2010), potentially reflecting a similar source area or provenance for both units in the Easton and Franciscan systems.

The magmatic arc of the Coast Plutonic Complex (also named the Coast Mountain Batholith) in Alaska and British Columbia (Gehrels et al., 2009; Cecil et al., 2021) could also be

a likely provenance for many of the Late-Jurassic-Early Cretaceous zircon grains from the Easton. The Coast Mountain Batholith in north-central BC has been split into two belts, an older western belt and a slightly younger eastern belt. Magmatism occurred in the western belt in 3 stages, from ~177 – 162 Ma, ~157 – 142 Ma, and ~118 – 100 Ma, with a recognizable magmatic lull from ~142 - 123 Ma (Gehrels et al., 2009). Magmatism in the eastern belt of the CPC has a similar signature to the western belt with the notable exception that there is a record of continuous magmatism from ~140 to ~120 Ma (Gehrels et al., 2009; Cecil et al., 2021). Similar Late Jurassic zircons in the Chugach accretionary complex have also been attributed to being sourced from the Coast Plutonic Complex (Amato et al., 2013). Because the eastern belt of the Coast Plutonic Complex has a continuity of zircon ages in the same age ranges recorded in the metasedimentary units in the Easton (Fig. 22), it is perhaps the most likely source arc for the detrital zircons analyzed in this study.

5.4 Causes of Subduction Accretion along the North American Margin

Subduction and accretion of metasedimentary units along the margin of western North America in the Jurassic and Cretaceous has been linked to changes in relative plate motion with implications for Cordilleran-wide tectonic events (Fig. 22). The metamorphic and detrital ages of subducted rocks from the Franciscan complex in California have been used to argue that the Franciscan subduction complex changed from a period of prolonged subduction erosion to subduction accretion circa 123 Ma (Dumitru et al., 2010). This time coincides with a proposed change in the direction and velocities of the North American and Pacific/Farallon plates (e.g., Engebretson et al., 1985), increased shortening in the Cordilleran forearc and retroarc (e.g., DeCelles et al., 2009), and transition from a magmatic lull to voluminous arc magmatism in the

Sierran batholith (Armstrong and Ward, 1993; DeGraaff-Surpless et al., 2002) (Fig. 22). Dumitru et al. (2010) postulated that the change in Pacific plate motions at ~123 Ma may have driven a transition from subduction erosion to subduction accretion, or conversely, that subduction accretion was driven by increased sediment supply from the continental margin.

The geochronology from the Easton metamorphic suite in this study suggests that subduction accretion began nearly 30 m.y. earlier than within the Franciscan complex further south along the Cordilleran margin (Fig. 22). The maximum depositional ages of the Darrington phyllite and Mt. Josephine semi-schist indicate that deposition of the sedimentary units likely occurred from at least 152 - 122 Ma, with subduction accretion following soon thereafter. Based on the youngest metamorphic constraints on the Mt. Josephine semi-schist (Misch, 1963) and fossil constraints from the rocks in San Juan Islands that have also undergone HP/LT metamorphism (Brown et al., 2005), continued subduction accretion of metasedimentary units within the NWCS persisted until at least ~115-112 Ma (Brown, 2012).

The earlier record of subduction accretion in the Easton metamorphic suite compared to the Franciscan suggests local tectonic settings and sediment supply more likely contributed to the onset of subduction accretion. If a change in plate motion were the primary driving mechanism, then one would expect to see synchronous changes along the continental margin, assuming a simple plate boundary geometry. In addition, for modern plate margins, the dominant control on whether a subduction zone experiences subduction erosion or subduction accretion is the amount of sediment supply with high amounts of sedimentation leading to subduction accretion (e.g., Scholl and von Huene, 2007).

6. CONCLUSIONS

Field mapping, structural analysis, and zircon U-Pb geochronology show that previously correlated units within the Easton metamorphic suite are instead distinct structural litho-tectonic units. From youngest to oldest these include the Mt Josephine semi-schist, the Darrington phyllite, and Shuksan greenschist. Based on the zircon results, it is possible that the Mt. Josephine semi-schist has at least two sets of maximum depositional ages at ~144 Ma and ~122 Ma and suggests different sources within the same unit or that the Mt Josephine semi-schist consists of units accreted at separate times. The Lummi formation in the NWCS yields similar maximum depositional ages as the older portions of the Mt Josephine semi-schist and may be correlative. In contrast, the Darrington phyllite could potentially be as much as 8 m.y. older than the oldest portion of the Mt. Josephine semi-schist and the youngest Mt. Josephine maximum depositional ages are younger than white mica $^{40}Ar/^{39}Ar$ ages of the Darrington phyllite. The Shuksan greenschist has a protolith age of 166 Ma but the structural and metamorphic history is different from the Darrington phyllite and the two units should be considered separately. Subduction accretion in the Easton metamorphic suite occurred ~30 m.y. earlier than the main accretionary phase in the Franciscan, suggesting that proposed changes in the relative Pacific and North American plate motion did not solely drive changes from subduction erosion to subduction accretion.

7. FUTURE WORK

Future work could involve gathering more U-Pb zircon samples from other outcrops of the Darrington phyllite, Mt. Josephine semi-schist, and Shuksan greenschist within the study area to fill in possible age gaps within the results. Preliminary work to find zircons within the amphibolite units of the metamorphic sole has already been accomplished; zircon ages from these earlier, high-

grade units near the Iron Mountain (Finney Creek) area could further contextualize the ages reported in this study. An examination of trace and Rare Earth Elements and Lu/Hf isotopes within Easton zircons could likely provide additional information on provenance and sourcing of the units to an even more refined extent. Pressure and temperature pseudosection modeling of rocks sampled at unit boundaries within the high grade metamorphic sole and the regional blueschist units would supplement the existing geochronological framework to confirm the structural relationship of contacts within the Easton units. Further sampling and detailed mapping of the differences between the Darrington phyllite and the Mt. Josephine semi-schist is needed to highlight the growing distinctions between these once correlated units. No published $^{40}Ar/^{39}Ar$ ages are currently available for the Mt. Josephine unit; to further constrain the outstanding differences of the Mt. Josephine and Darrington units identified in this work, gathering samples for $^{40}Ar/^{39}Ar$ geochronology from the study areas would be a logical next target for future research.

REFERENCES CITED

Allmendinger, R.W., Siron, C.R., and Scott, C.P., 2017, Structural data collection with mobile devices: Accuracy, redundancy, and best practices: Journal of Structural Geology, v. 102, p. 98–112, doi:10.1016/j.jsg.2017.07.011.

Amato, J. M., Pavlis, T. L., Clift, P. D., Kochelek, E. J., Hecker, J. P., Worthman, C. M., and Day, E. M., 2013, Architecture of an accretionary complex as revealed by detrital zircon ages and lithologic variations: Evidence for subduction erosion in the Mesozoic Chugach terrane, southern Alaska, Geological Society of America Bulletin, v. 125, p. 1891-1911, doi:10.1130/B30818.1.

Apen, F.E., Wakabayashi, J., Day, H.W., Roeske, S.M., Souders, A.K., Dumitru, T.A., 2021, Regional-scale correlations of accreted units in the Franciscan Complex, California, USA: A record of long-lived, episodic subduction accretion, *in* Wakabayashi, J., and Dilek, Y., eds., Plate Tectonics, Ophiolites, and Societal Significance of Geology: A Celebration of the Career of Eldridge Moores: Geological Society of America Special Paper 552, p. 233–255, https://doi.org/ 10.1130/2021.2552(11).

Armstrong, R.L., 1980, Geochronometry of the Shuksan Metamorphic Suite, North Cascades, Washington: Geological Society of America Abstracts with Programs, v. 12 no. 3, p. 94.

Armstrong, R. L., and Ward, P.L., 1993, Late Triassic to earliest Eocene magmatism in the North American Cordillera: Implications for the Western Interior Basin, *in* Evolution of the Western Interior Basin, edited by W. G. E. Caldwell and E. G. Kauffman, Geological Association of Canada Special Paper, 39, p. 49–72.

Brandon, M.T., Cowan, D.S., and Vance, J.A., 1988, The Late Cretaceous San Juan thrust system, San Juan Islands, Washington: Geological Society of America Special Paper 221, 81 pp.

Brown, E.H. 1977, Ophiolite on Fidalgo island, Washington, *In* North American ophiolites, *Eds:* R.G. Coleman and W.P. Irwin. Oregon Department of Geology and Mineral Industries, Bulletin 95, p. 67–93.

Brown, E.H., Wilson, D.L., Armstrong, R.L., and Harakal, J.E., 1982, Petrologic, structural, and age relations of serpentinite, amphibolite, and blueschist in the Shuksan Suite of the Iron Mountain-Gee Point area, North Cascades, Washington: GSA Bulletin, v. 93, p. 1087–1098, doi: 10.1130/0016-7606(1982)93<1087:PSAARO>2.0.CO;2.

Brown, E.H., 1986, Geology of the Shuksan Suite, North Cascades, Washington, USA: Geological Society of America Memoirs, v. 164, p. 143–154.

Brown, E.H., 1987, Structural geology and accretionary history of the Northwest Cascades system, Washington and British Columbia: Geological Society of America Bulletin, v. 99, p. 201–214, doi: 10.1130/0016-7606(1987)99<201:SGAAHO>2.0.CO;2.

Brown, E. H., and Blake, M. C., Jr., 1987, Correlation of Early Cretaceous blueschists in Washington, Oregon, and northern California: Tectonics, v. 6, p. 795-806.

Brown, E.H., Lapen, T.J., Leckie, R.M., Premoli Silva, I., Verge, D., and Singer, B.S. 2005. Revised ages of blueschist metamorphism and the youngest pre-thrusting rocks in the San Juan Islands, Washington: Canadian Journal of Earth Sciences, v. 42(7), p. 1389–1400.

Brown, E.H., and Gehrels, G.E., 2007, Detrital zircon constraints on terrane ages and affinities and timing of orogenic events in the San Juan Islands and North Cascades, Washington: Canadian Journal of Earth Sciences, v. 44, p. 1375–1396, doi:10.1139/E07-040.

Brown, E.H., 2012, Obducted nappe sequence in the San Juan Islands – northwest Cascades thrust system, Washington and British Columbia: Canadian Journal of Earth Sciences, v. 49, p. 796– 817, doi: 10.1139/e2012-026.

Burmester, R.F., Blake, M.C., Jr, and Engebretson, D.C., 2000, Remagnetization during Cretaceous Normal Superchron in Eastern San Juan Islands, WA: implications for tectonic history: Tectonophysics, v. 326 (1–2), p. 73–92, doi:10.1016/S0040-1951(00)00147-5.

Cawood, P.A., Hawkesworth, C.J., Dhuime, B., 2012, Detrital zircon record and tectonic setting: Geology, v. 40 (10), p. 875–878. doi: https://doi.org/10.1130/G32945.1.

Cecil, M.R., Gehrels, G.E., Rusmore, M.E., Woodsworth, G.J., Stowell, H.H., Yokelson, I.N., Homan, E., Kitajima, K., and Valley, J.W., 2021, Mantle control on magmatic flare-ups in the southern Coast Mountains batholith, British Columbia: Geosphere, v. 17, p. 1–15, https://doi.org/10.1130 /GES02361.1.

Cordova, J.L., Mulcahy, S.R., Schermer, E.R., and Webb, L.E., 2018, Subduction initiation and early evolution of the Easton metamorphic suite, northwest Cascades, Washington: Lithosphere, v. 11, p. 44–58.

Coutts, D. S., Matthews, W. A., & Hubbard, S. M., 2019, Assessment of widely used methods to derive depositional ages from detrital zircon populations: Geoscience Frontiers, v. 10, p. 1421-1435, doi:10.1016/j.gsf.2018.11.002.

DeCelles, P.G., Ducea, M.N., Kapp, P., and Zandt, G., 2009, Cyclicity in Cordilleran orogenic systems: Nature Geoscience, v. 2, p. 251–257, doi:10.1038/ngeo469.

DeGraaff-Surpless, K., Graham, S.A., Wooden, J.L., and McWilliams, M.O., 2002, Detrital zircon provenance analysis of the Great Valley Group, California: Evolution of an arc-forearc system: Geological Society of America Bulletin, v. 114, p. 1564–1580. doi:10.1130/0016-7606 (2002)114<1564:DZPAOT>2.0.CO;2.

Dickinson, W. R., and Gehrels, G. E., 2009). Use of U–Pb ages of detrital zircons to infer maximum depositional ages of strata: A test against a Colorado Plateau Mesozoic database: Earth and Planetary Science Letters, v. 288, p. 115–125, doi:10.1016/j.epsl.2009.09.013.

Dragovich, J.D., Norman, D.K., Grisamer, C.L., Logan, R.L., and Anderson, G., 1998, Geologic Map and Interpreted Geologic History of the Bow and Alger 7.5 Minute Quadrangles, Western Skagit County, Washington: Washington Division of Geology and Earth Resources Open-File Report 98–5, 80 p., 3 plates.

Dragovich, J.D., Norman, D.K., and Anderson, G., 2000, Interpreted Geologic History of the Sedro-Woolley North and Lyman 7.5-Minute Quadrangles, Western Skagit County, Washington: Washington Division of Geology and Earth Resources Open-File Report 2000–1, 71 p., 1 plate.

Dungan, M.A., Vance, J.A., and Blanchard, D.P., 1983, Geochemistry of the Shuksan greenschists and blueschists, North Cascades, Washington: Variably fractionated and altered metabasalts of oceanic affinity: Contributions to Mineralogy and Petrology, v. 82, p. 131–146, doi:10.1007/BF01166608.

Dumitru, T.A., Wakabayashi, J., Wright, J.E., Wooden, J.L., 2010, Early Cretaceous transition from nonaccretionary behavior to strongly accretionary behavior within the Franciscan subduction complex: Tectonics, v. 29, TC5001. https://doi.org/10.1029/ 2009TC002542.

Dumitru, T. A., Ernst, W. G., Hourigan, J. K., and McLaughlin, R. J., 2015, Detrital zircon U–Pb reconnaissance of the Franciscan subduction complex in northwestern California: International Geology Review, v. 57 (5–8), p. 767–800. https://doi.org/10.1080/00206814.2015.1008060.

Dumitru, T.A., Hourigan, J.K., Elder, W.P., Ernst, W.G., and Joesten, R., 2018, New, much younger ages for the Yolla Bolly terrane and a revised timeline for accretion in the Franciscan subduction complex, California: *in* Tectonics, Sedimentary Basins, and Provenance: A Celebration of the Career of William R. Dickinson, Raymond V. Ingersoll, Timothy F. Lawton, Stephan A. Graham: GSA Special Papers, v. 540.

Engebretson, D. C., Cox, A., and Gordon, R. G., 1985, Relative motions between oceanic and continental plates in the Pacific Basin: Geological Society of America Special Paper 206, 59 pp.

Gallagher, M.P., Brown, E.H., and Walker, N.W., 1988, A new structural and tectonic interpretation of the western part of the Shuksan blueschist terrane, northwestern Washington: Geological Society of America Bulletin, v. 100, p. 1415–1422, doi: 10.1130/0016- 7606(1988)100<1415:ANSATI>2.3.CO;2.

Gehrels, G.E., Valencia, V., Ruiz, J., 2008, Enhanced precision, accuracy, efficiency, and spatial resolution of U-Pb ages by laser ablation-multicollector-inductively coupled plasma-mass spectrometry: Geochemistry, Geophysics, Geosystems, v. 9, Q03017, doi:10.1029/2007GC001805.

Gehrels, G., Rusmore, M., Woodsworth, G., Crawford, M., Andronicos, C., Hollister, L., Patchett, J., Ducea, M., Butler, R., Klepeis, K., Davidson, C., Friedman, R., Haggart, J., Mahoney, B., Crawford, W., Pearson, D., and Girardi, J., 2009, U-Th-Pb geochronology of the Coast Mountains batholith in north coastal British Columbia: Constraints on age and tectonic evolution: Geological Society of America Bulletin, v. 121, no. 9–10, p. 1341–1361, https://doi.org/10.1130/B26404.1.

Gehrels, G. and Pecha, M., 2014, Detrital zircon U-Pb geochronology and Hf isotope geochemistry of Paleozoic and Triassic passive margin strata of western North America: Geosphere, v. 10 (1), p. 49-65.

Gusey, D.L., 1978, The geology of southwestern Fidalgo Island [M.S. thesis]: Western Washington University.

Hampton, B. A., Ridgway, K. D., & Gehrels, G. E. (2010). A detrital record of Mesozoic island arc accretion and exhumation in the North American Cordillera: U-Pb geochronology of the Kahiltna basin, southern Alaska. Tectonics, v. 29 (4), 21 p., doi:10.1029/2009tc002544.

Haugerud, R.A., Morrison, M.L., and Brown, E.H., 1981, Structural and metamorphic history of the Shuksan Metamorphic Suite in the Mount Watson and Gee Point areas, North Cascades, Washington: Geological Society of America Bulletin, v. 92, p. 374-383.

Kalbas, J. L., Ridgway, K. D., & Gehrels, G. E., 2007, Stratigraphy, depositional systems, and provenance of the Lower Cretaceous Kahiltna assemblage, western Alaska Range: Basin development in response to oblique collision: The Geological Society of America Special Paper 431: Tectonic Growth of a Collisional Continental Margin: Crustal Evolution of Southern Alaska, p. 307–343, doi:10.1130/2007.2431(13).

Lamb, W.M., 2000, Structural and Tectonic History of the Eastern San Juan Islands, Washington, [MS Thesis]: Western Washington University, 270 p.

MacDonald, J.H., Jr., and Dragovich, J.D., 2015, Sedimentary geochemistry of the Peshastin Formation and Darrington Phyllite, Cascade Mountains, Washington State: Provenance, tectonic setting, and regional implications, in Anderson, T.H., Didenko, A.N., Johnson, C.L., Khanchuk, A.I., and MacDonald, J.H., Jr., eds., Late Jurassic Margin of Laurasia—A Record of Faulting Accommodating Plate Rotation: Geological Society of America Special Paper 513, p. 441–460, https://doi.org/10.1130/2015.2513(12).

Misch, P., 1963, New samples for age determinations from the Northern Cascades, in Kulp, J.L., Senior investigator, and others, Investigations in isotopic geochemistry: Columbia University, Lamont Geological Observatory (U.S. Atomic Energy Commission [Pub.] NYO7243), Report 8, p. 26–40, App. K, p. 1–4.

Misch, P., 1964, Age determinations of crystalline rocks of northern Cascade Mountains, in Kulp, J.L., Senior investigator, and others, Investigations in isotopic geochemistry: Columbia

University, Lamont Geological Observatory (U.S. Atomic Energy Commission [Pub.] NYO7243), Report 9, App. D, p. 1–15.

Misch, P., 1966, Tectonic evolution of the northern Cascades of Washington State, *in* Gunning, H.C., ed., Symposium on the Tectonic History and Mineral Deposits of the Western Cordillera in British Columbia and Neighboring Parts of the United States: Canadian Institute of Mining and Metallurgy Special Publication 8, p. 101–148.

Orme, D.A., and Surpless, K.D., 2019, The birth of a forearc: The basal Great Valley Group, California, USA: Geology, v. 47, p. 757–761, doi.org/10.1130/G46283.1

Roser, B.P., and Korsch, R.J., 1986, Determination of tectonic setting of sandstone–mudstone suites using SiO_2 content and K_2O/Na_2O ratio; Journal of Geology, v. 94 (5), p. 635–650.

Saleeby, J.B., 1996, Coast Range ophiolite as parautochthonous forearc lithosphere: GSA Today, v. 6, no. 2, p. 6–8.

Sauer, K.B., Gordon, S. M., Miller, R. B, Vervoort, J. D., and Fisher, C. M., 2017, Evolution of the Jura-Cretaceous North American Cordilleran margin: Insights from detrital-zircon U-Pb and Hf isotopes of sedimentary units of the North Cascades Range, Washington: Geosphere, v. 13 (6), p. 2094–2118. Doi: https://doi.org/10.1130/GES01501.1.

Schermer, E.R., Gillaspy, J.R., and Lamb, R., 2007, Arc-parallel extension and fluid flow in an ancient accretionary wedge: The San Juan Islands, Washington: Geological Society of America Bulletin, v. 119, no. 5–6, p. 753–767, https://doi.org/10.1130/B25985.1.

Schermer, E.R., Hoffnagle, E.A., Brown, E.H., Gehrels, G.E., and McClelland, W.E., 2018, U-Pb and Hf isotopic evidence for an Arctic origin of terranes in northwestern Washington: Geosphere; 14 (2): 835–860. doi: https://doi.org/10.1130/GES01557.1.

Scholl, D. W., and R. von Huene, 2007, Crustal recycling at modern subduction zones applied to the past: Issues of growth and preservation of continental basement crust, mantle geochemistry, and supercontinent reconstruction, in 4-D Framework of Continental Crust, edited by R. D. Hatcher Jr. et al., Geological Society of America Memoirs, v. 200, p. 9–32, doi:10.1130/2007.1200(02).

Sharman, G.R., Sharman, J.P., and Sylvester, Z., detritalPy: A Python-based toolset for visualizing and analysing detrital geo-thermochronologic data: Depositional Record, v. 4, p. 202– 215. https://doi.org/10.1002/dep2.45.

Shervais, J.W., 2001, Birth, death and resurrection: The life cycle of suprasubduction zone ophiolites: Geochemistry, Geophysics, Geosystems, v. 2, 1010, https://doi.org/10.1029/2000GC000080.

Snow, C. A., Wakabayashi, J., Ernst, W. G., & Wooden, J. L., 2010, Detrital zircon evidence for progressive underthrusting in Franciscan metagraywackes, west-central California: Geological Society of America Bulletin, v. 122, p. 282 – 291.

Street-Martin, L. V., 1981, The Chemical Composition of the Shuksan Metamorphic Suite in the Gee Point - Finney Creek Area, North Cascades, Washington [M.S. Thesis]: Western Washington University, 102 p.

Tabor, R.W., Booth, D.B., Vance, J.A., and Ort, M.H., 1988, Preliminary Geologic Map of the Sauk River 30 × 60 Minute Quadrangle, Washington: U.S. Geological Survey Open-File Report 88–692, with pamphlet, 50 p., scale 1:100,000.

Tabor, R.W., 1994, Late Mesozoic and possible early Tertiary accretion in western Washington State: The Helena-Haystack mélange and the Darrington-Devils Mountain fault zone: Geological Society of America Bulletin, v. 106, p. 217–232.

Tabor, R. W.; Booth, D. B.; Vance, J. A.; Ford, A. B., 2002, Geologic map of the Sauk River 30-by 60-minute quadrangle, Washington: U.S. Geological Survey Geologic Investigations Series Map I-2592, 2 sheets, scale 1:100,000, with 67 p. text.

Tabor, R.W., Haugerud, R.A., Hildreth, W., and Brown, E.H., 2003, Geologic Map of the Mount Baker 30 by 60 Minute Quadrangle, Washington: U.S. Geological Survey Geologic Investigation Series Map I-2660, with pamphlet, 70 p., scale 1:100,000.

Vance, J.A., 1975, Bedrock geology of San Juan County, IN Russel, R.H., ed., Geology and Water Resources of the San Juan Islands, San Juan County, Washington: Washington Department of Ecology Water-Supply Bulletin, no. 46, p. 3-19, (incl. geologic map, scale 1:63,360).

Vermeesch, P., 2018, IsoplotR: a free and open toolbox for geochronology: Geoscience Frontiers, v. 9, p. 1479–1493: https://doi.org/10.1016/j.gsf.2018.04.001.

Washington Division of Geology and Earth Resources, 2016, Surface geology, 1:100,000--GIS data, November 2016: Washington Division of Geology and Earth Resources Digital Data Series DS-18, version 3.1.

FIGURES

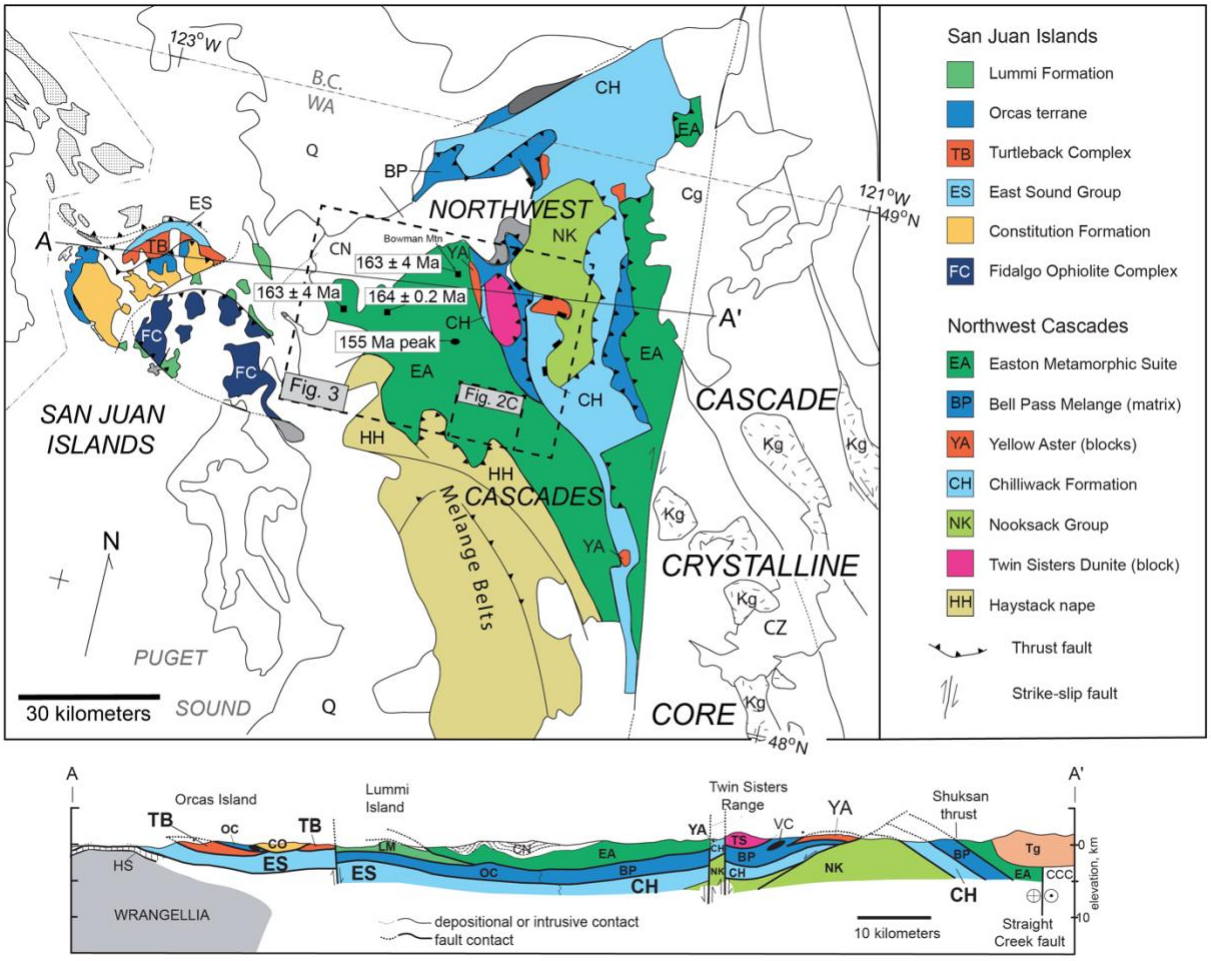

Figure 1. Geologic map and cross section of the Northwest Cascades Thrust System (NWCS) nappe sequence including the subduction zone rocks of the Easton metamorphic suite (EA) in green. Study areas outlined by dashed boxes and represent the extent of Figures 2C and 3. Map from Schermer et al. (2018). Previous U-Pb geochronology in the Easton metamorphic suite includes ages from Dragovich et al. (1998), Gallagher et al. (1988), and Brown and Gehrels (2007). Black squares are igneous U-Pb ages, and the black oval is the single U-Pb detrital zircon age for the Mt. Josephine before this study.

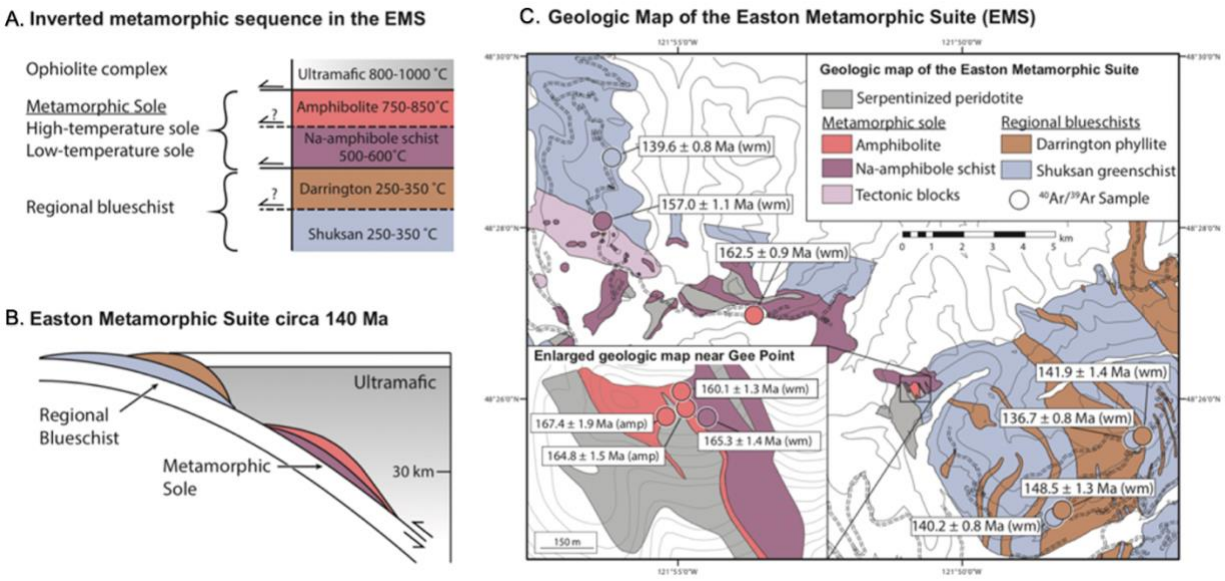

Figure 2. A) Composite inverted metamorphic sequence in the Easton metamorphic suite, showing decreasing temperature with depth and possible fault relationships between units. B) Schematic cross-section of the Easton metamorphic suite during subduction, circa 140 Ma. C) Geologic map of the Easton metamorphic suite near Iron Mountain and Gee Point, Washington, with $^{40}Ar/^{39}Ar$ ages from Cordova et al. (2018). Abbreviations: amp, amphibole; wm, white mica. Modified from Cordova et al. (2018).

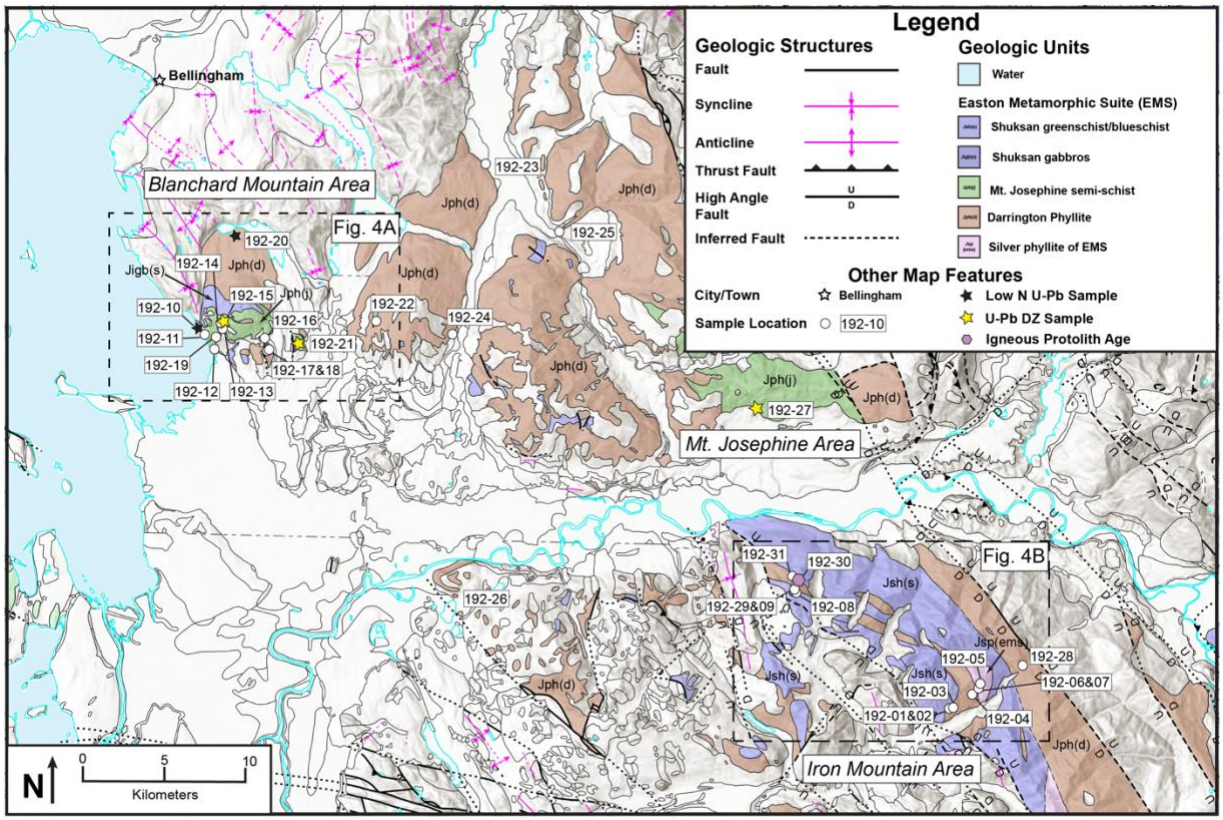

Figure 3. Geologic map of the Easton metamorphic suite, with sample locations for this study in white circles and U-Pb zircon geochronology samples in yellow squares. Dashed boxes show the extent of Fig. 4A and B. The three main study areas discussed in the text are labeled. All GIS data obtained from the Washington state Department of Natural Resources geology portal (find here: https://fortress.wa.gov/dnr/geologydata/publications/data_download/ger_portal_surface_geology_100k.zip).

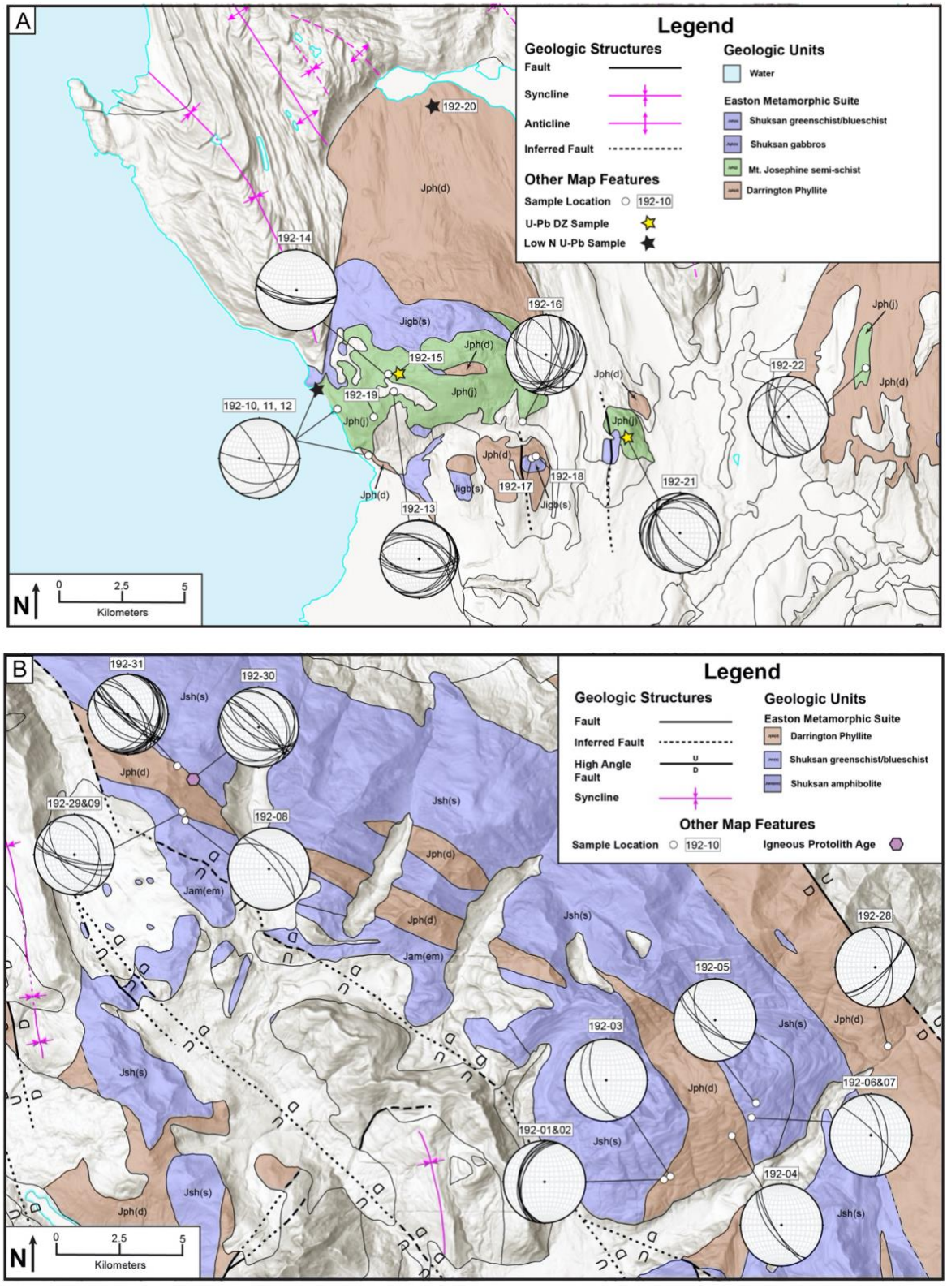

Figure 4. A) Stereograms of foliation planes in the Blanchard Mountain study area. B) Stereograms of foliation planes in the Iron Mountain study area from Figure 3.

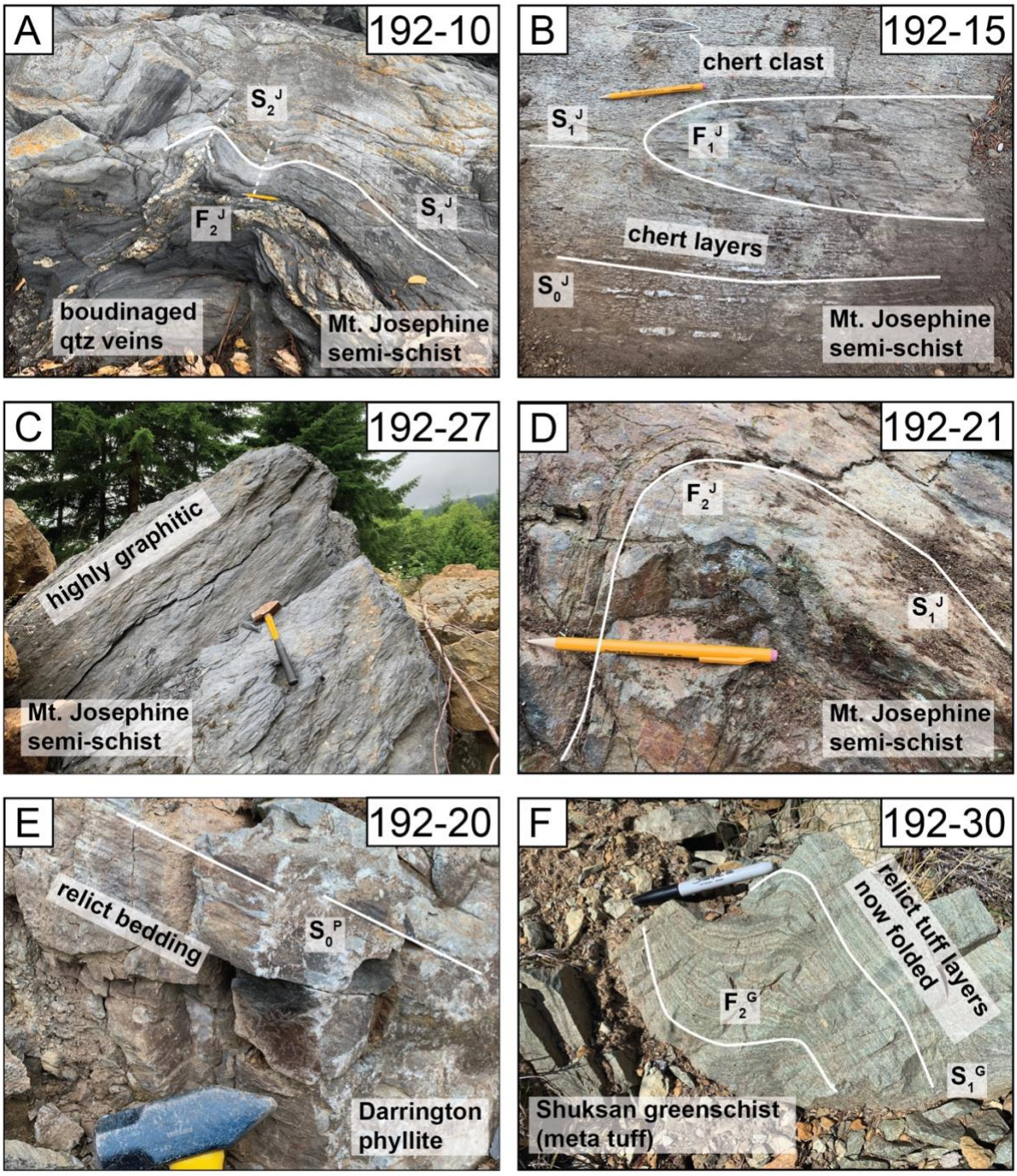

Figure 5. Field photographs of all U-Pb zircon geochronology samples in this study. Structural features of note are outlined in white, with geologic unit and sample number labeled. Sense of scale is shown using a pencil, pen, or hammer. A) A coarse Mt. Josephine semi-schist from the Blanchard Mountain study area with second generation folds (F_2^J), an S_1^J fabric folded by the F_2^J event, and a weak axial planar fabric (S_2^J) more easily identified in thin section indicated by the dotted white lines. Boudinaged quartz veins are parallel to the S_1^J fabric and commonly are associated with the F_2^J folds. B) A rare F_1^J fold and the axial

planar S_1^J fabric in the Mt. Josephine semi-schist. Meta-chert clasts and layers that are sub-parallel to the F_1^J fold and the S_1^J fabric are also labelled. C) A graphitic version of the Mt. Josephine semi-schist unit from the Mt. Josephine study area. D) The S_1^P fabric is folded by the F_2^P folds in the Mt. Josephine semi-schist. E) Relict bedding (S_0^P) in the Darrington phyllite that is parallel to S_1^P. F) Tuffaceous layers in the Shuksan greenschist from the Iron Mountain study area. The S_1^G fabric is folded by the F_2^G.

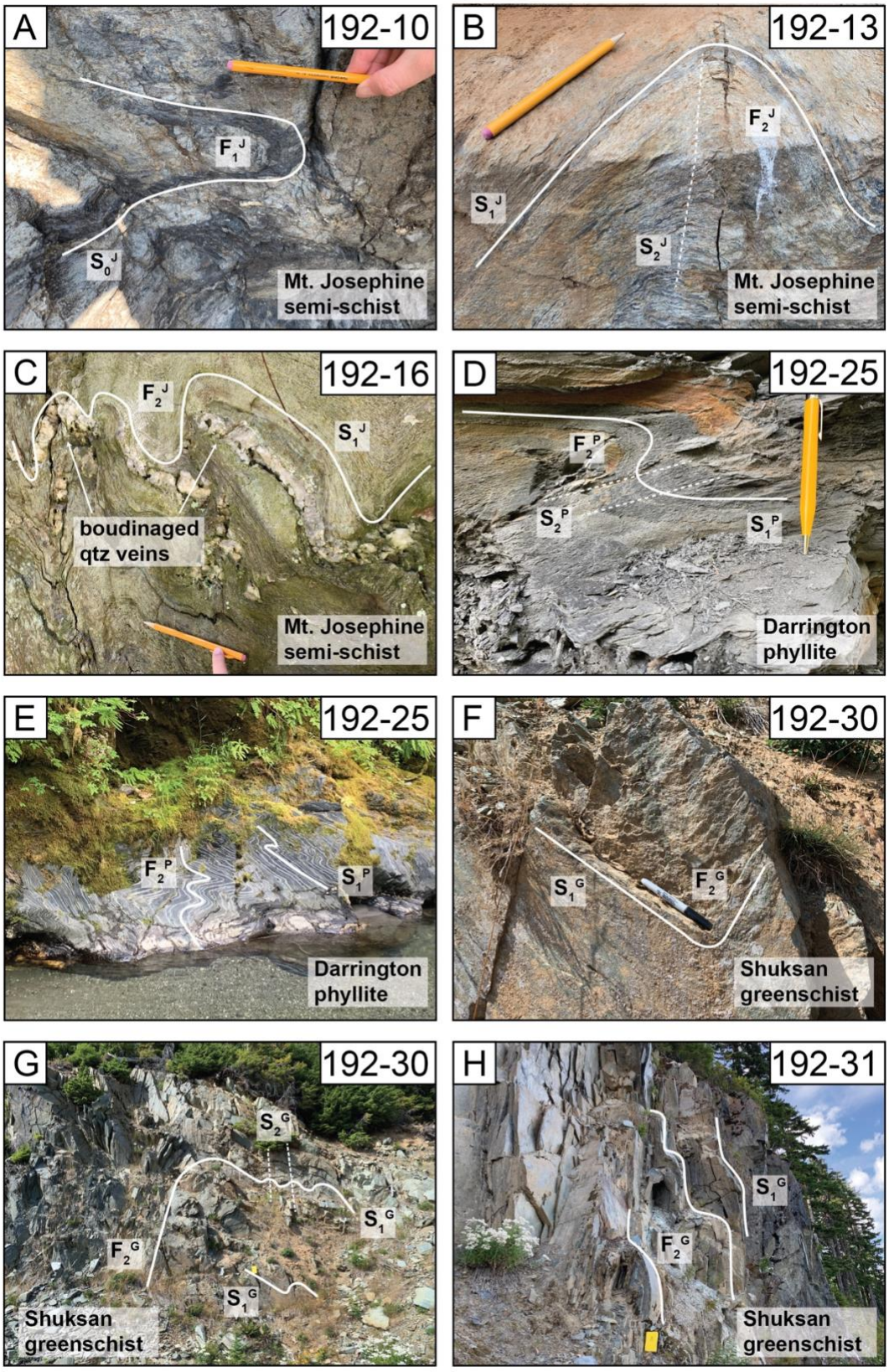
A
192-10
F_1^J
S_0^J
Mt. Josephine semi-schist
B
192-13
F_2^J
S_1^J
S_2^J
Mt. Josephine semi-schist
C
192-16
F_2^J
S_1^J
boudinaged qtz veins
Mt. Josephine semi-schist
D
192-25
F_2^P
S_2^P
S_1^P
Darrington phyllite
E
192-25
F_2^P
S_1^P
Darrington phyllite
F
192-30
S_1^G
F_2^G
Shuksan greenschist
G
192-30
S_2^G
S_1^G
F_2^G
S_1^G
Shuksan greenschist
H
192-31
S_1^G
F_2^G
Shuksan greenschist

Figure 6. Field photos of outcrops with folds from sample localities in this study. Structural features of note are outlined in white, with geologic unit and sample number labeled. Sense of scale is shown using a pencil, pen, or field notebook. A) A rare F_1^J fold in the Mt. Josephine semi-schist is visible in the dark-gray layer and folds the relict bedding. B) The S_1^J fabric in the semi-schist is folded by F_2^J. C) Boudinaged quartz veins parallel the S_1^J fabric and are folded by F_2^J folds. D) The S_1^J fabric in the semi-schist is folded by F_2^J and is crosscut by an axial planar fabric (S_2^J) (white dashed lines). E) The S_1^P in the Darrington phyllite is folded by the dominant F_2^P folds. Approximate field of view is 6 meters. F) The S_1^G fabric of the Shuksan greenschist is folded by the F_2^G folds, which are the most dominant and common folds. G) The S_1^G fabric is folded by the second generation of folds (F_2^G) that have an axial planar fabric (S_2^G). H) An oblique outcrop view of the F_2^G folds and the folded S_1^G fabric in the Shuksan greenschist.

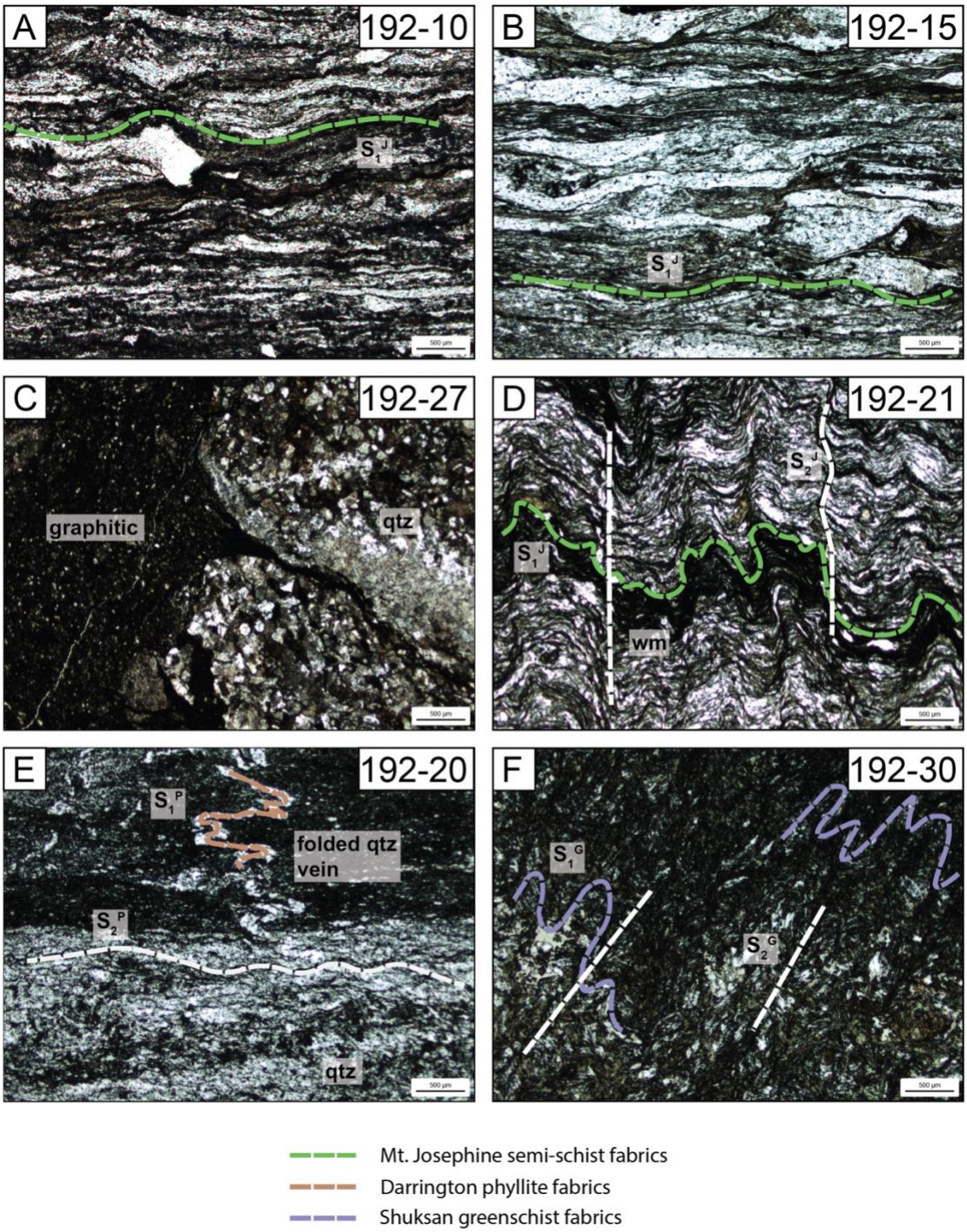

Figure 7. Thin section photomicrographs of the rocks sampled for U-Pb geochronology under cross-polarized light. Green lines represent Mt. Josephine semi-schist fabrics, brown lines represent Darrington phyllite fabrics, and purple lines represent Shuksan greenschist/blueschist fabrics. Qtz - quartz, Wm - white mica, Ab - albite, Chl- chlorite. A and B) Elongated chert clasts parallel to the S_1^J fabric in the Mt. Josephine

semi-schist. Note, these samples are coarser than that of the Darrington phyllite in photo E. C) Sample 192-27 with graphitic layers that surround chert clasts/layers. D) A poorly developed S_2^J axial planar crenulation cleavage weakly overprints an S_1^J fabric, that is parallel to S_0^J indicated by the finely crystalline white mica, coarser quartz, and graphite layering. E) A folded quartz vein (S_1^P) is overprinted by the axial planar S_2^P fabric in the Darrington phyllite, with much of the mineralogy being quartz and white mica. F) The S_1^G fabric from the Shuksan greenschist meta-tuff is weakly crosscut by the S_2^G axial planar fabric.

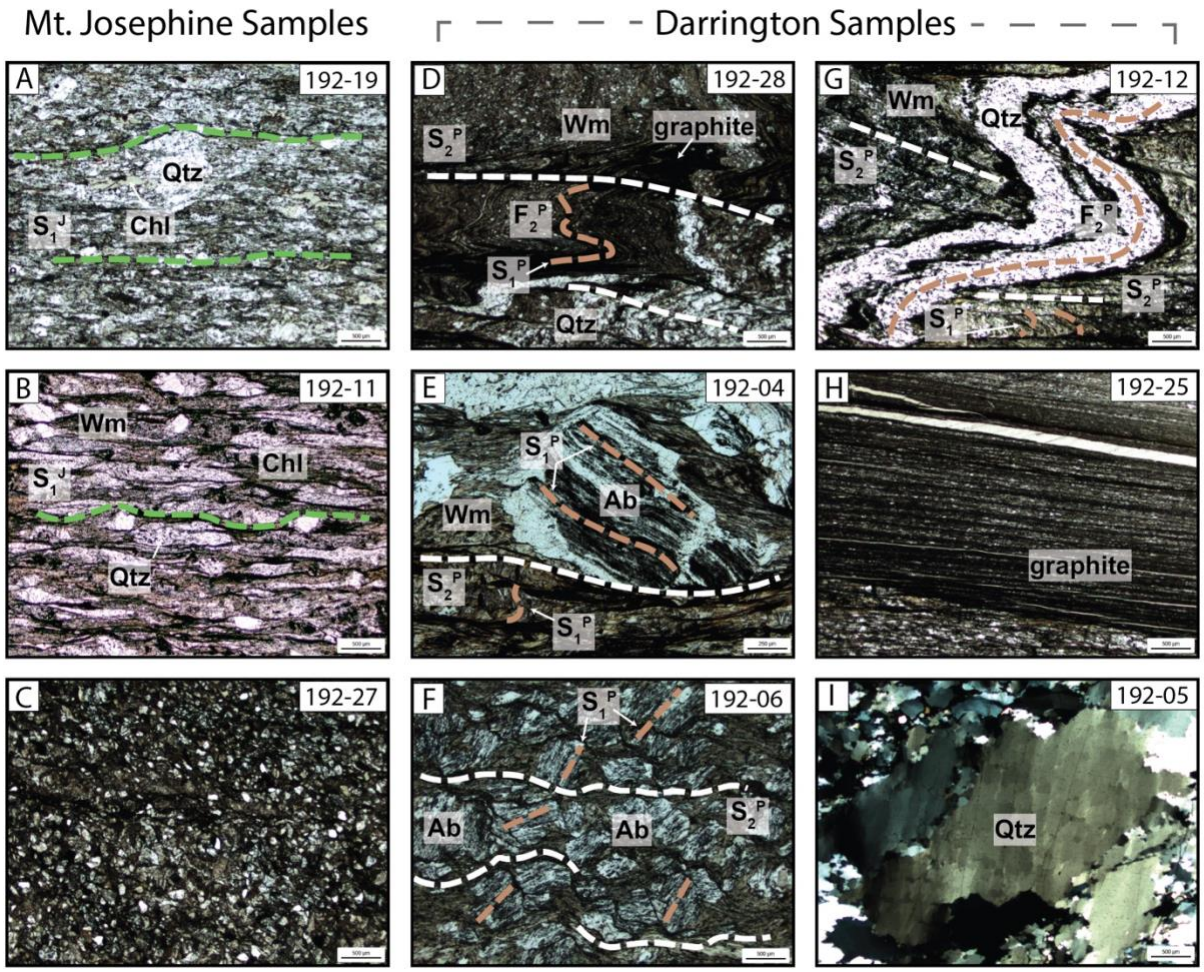

Figure 8. Thin section photomicrographs of the Mt. Josephine semi-schist samples on the left and Darrington phyllite samples on the right under cross-polarized light. Fabrics of the Mt. Josephine and Darrington delineated by dashed lines; green represents Mt. Josephine semi-schist, brown represents the Darrington phyllite. A, B) The S_1^J fabric in the Mt. Josephine semi-schist. C) The semi-schist from the Mt. Josephine study area is highly graphitic, has minor calcite, but does not have a well-developed fabric. D) The S_1^P fabric in the Darrington phyllite folded by the F_2^P folds and overprinted by the axial planar S_2^P fabric. E, F) Large, texturally zoned albites from the eastern exposures of the Darrington phyllite. The S_1^P fabric is preserved in the interior of the albite crystals and the S_2^P fabric in the surrounding matrix. G) The S_2^P fabric overprints the S_1^P fabric which is folded by F_2^P. H) Internal grain size difference within the Darrington in a graphitic area. I) A large quartz grain from the Darrington in the Iron Mountain study area showing undulose extinction and sub-grain recrystallization.

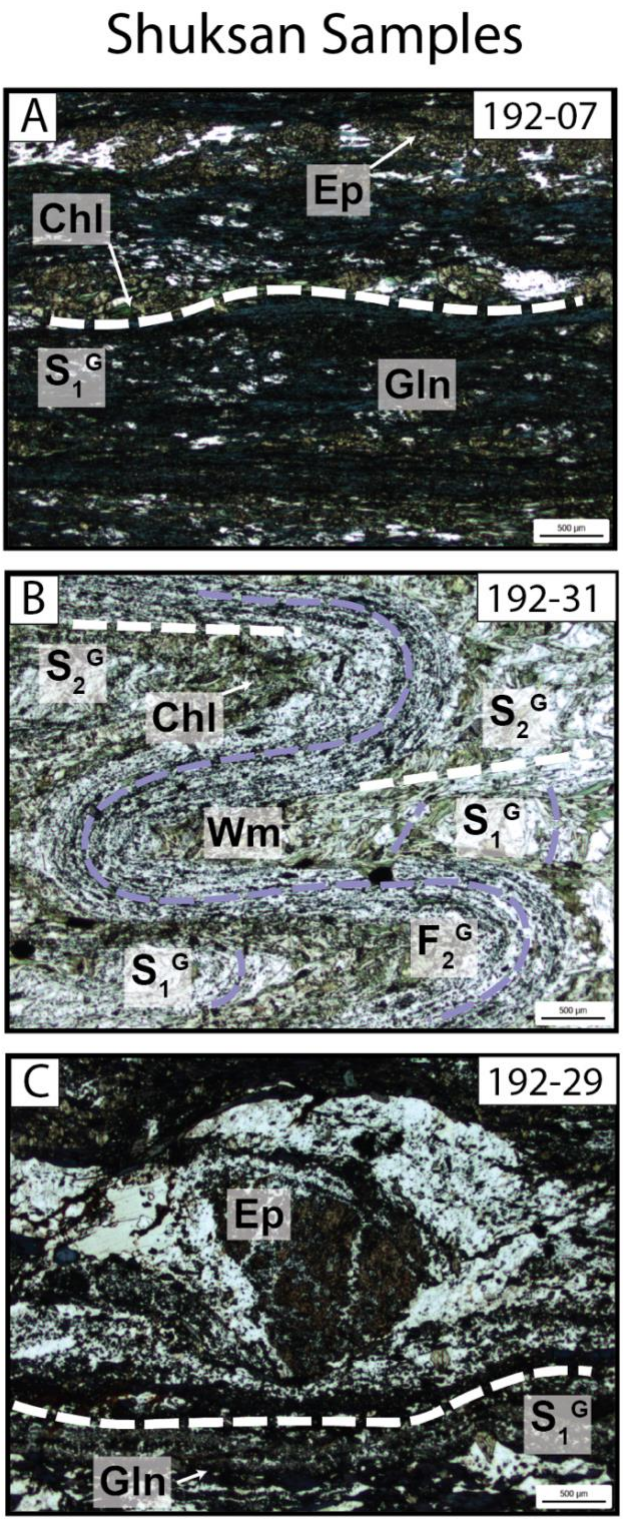

Figure 9. Thin section photomicrographs of the Shuksan greenschist/blueschist unit under cross-polarized light (A, C) and plane polarized light (B). Dashed purple lines represent the S_1^G fabric, and dashed white lines represent the S_2^G fabric. Minerals indicated by the abbreviations: Chl - chlorite, Gln - Glaucophane,

Wm - white mica, Ep - epidote. A) Greenschist and blueschist layering outlined by S_1^G is the dominant fabric in this sample, defined by chlorite and glaucophane. B) From the tuffaceous Shuksan sample, the S_1^G fabric (purple) is still preserved but is partially overprinted by the S_2^G fabric (white). C) The S_1^G fabric from the Shuksan in the Iron Mountain study area wraps around a large epidote crystal.

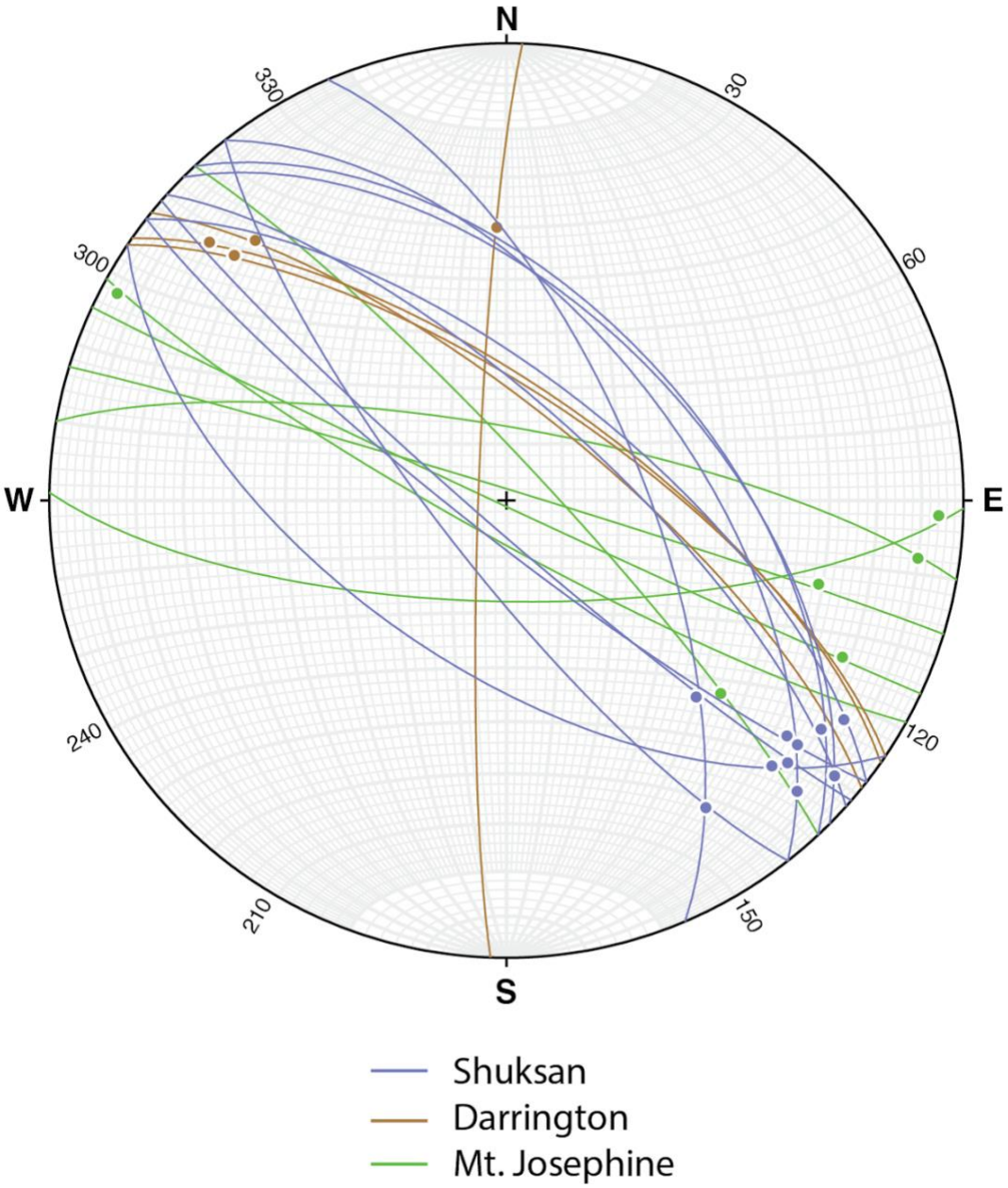

Figure 10. Stereonet plot of F_2 fold axial planes throughout the field area (great circles). Fold axes are plotted as the dots on each great circle and are divided by unit lithology (Shuksan, purple; Darrington, brown; Mt. Josephine, green).

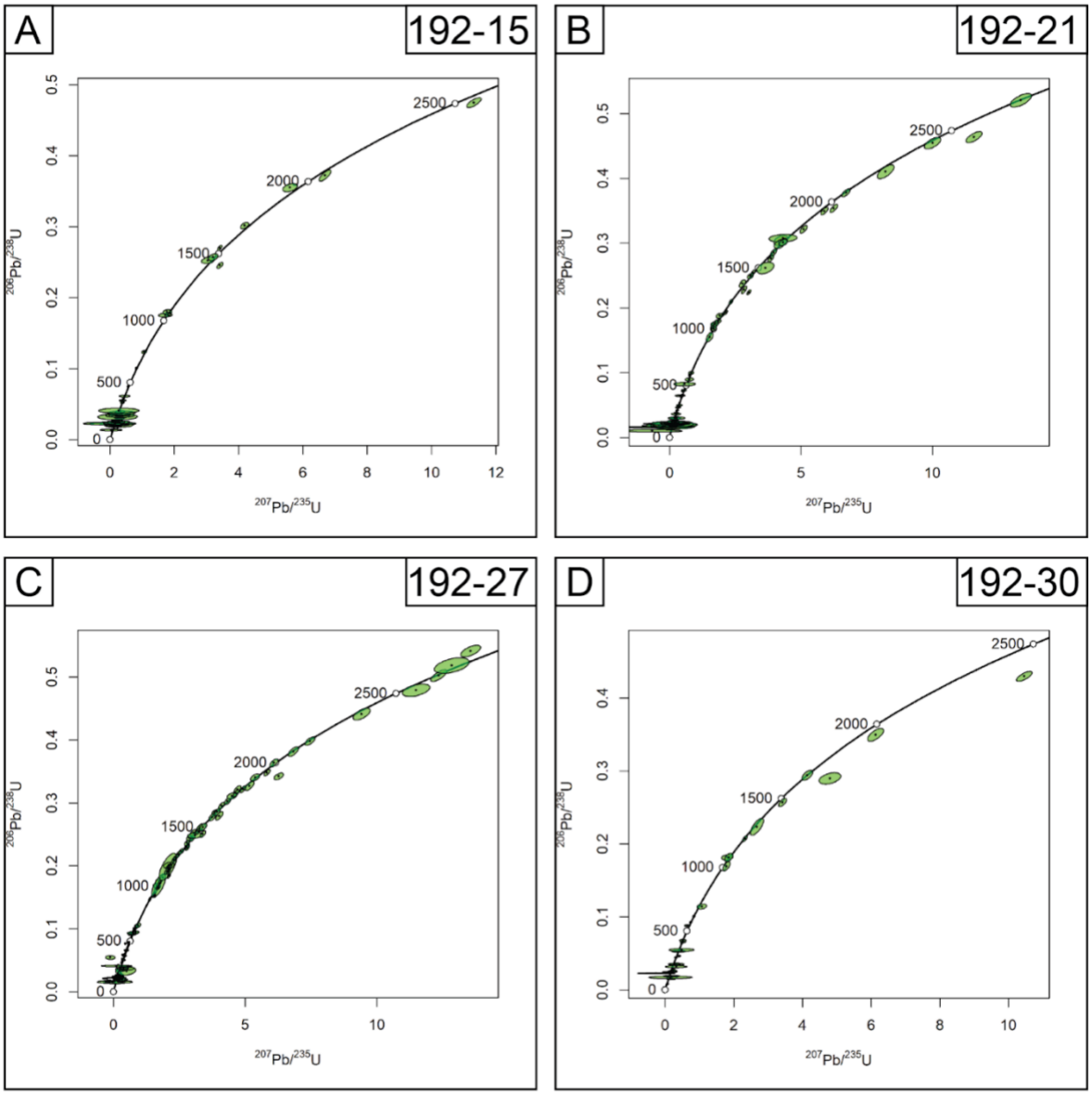

Figure 11. Wetherill-concordia plots for the four samples with a high zircon yield from this study. All grains plotted as green ellipses, including discordant grains. Analyses that are within 2σ uncertainty of the concordia line are considered concordant grains (A-C: Mt. Josephine samples 192-15, 192-21, 192-27, respectively; D) Shuksan greenschist sample 192-30). A) Mt. Josephine semi-schist (192-15) yielded a total of 239 grains, with 227 grains falling on the concordia line. B) Mt. Josephine semi-schist sample (192-21) yielded a total of 282 grains, with 266 falling on the concordia line. C) A highly graphitic Mt. Josephine semi-schist sample (192-27) yielded a total of 243 grains, with only 150 grains falling on the concordia line. D) The only Shuksan greenschist sample shows a total of 42 zircon grains, with 37 grains falling on the concordia line.

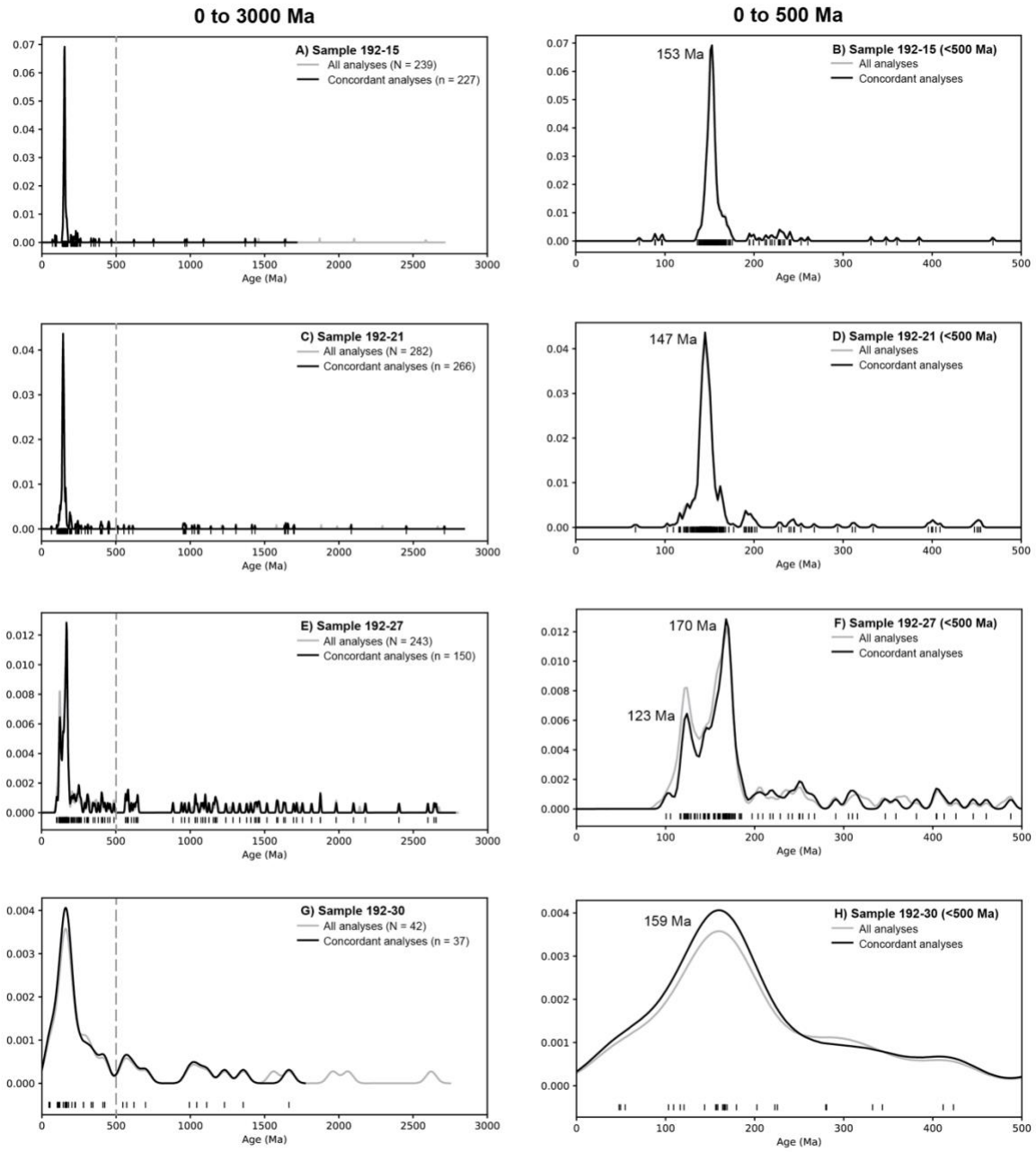

Figure 12. U-Pb zircon age distributions of samples from this study plotted as kernel density estimates (KDE) ranging from west to east as sample numbers increase. A-B) Mt. Josephine sample 192-15; C-D) Mt. Josephine sample 192-21; E-F) Mt. Josephine sample 192-27; G-H) Shuksan greenschist sample 192-30. The left column shows samples of this study from a 0 to 3000 Ma extent and the right column shows the same samples enlarged to show the extent from a 0 to 500 Ma. The dotted vertical line at 500 Ma indicates the extent for the KDE on the right column. For each sample, the KDE curve is plotted for all analyses (N, gray curve) and for analyses that are concordant within 2σ uncertainty (n, black curve). Small vertical ticks on X-axis represent each individual age analysis within the samples. Age peaks have been rounded to the nearest whole number.

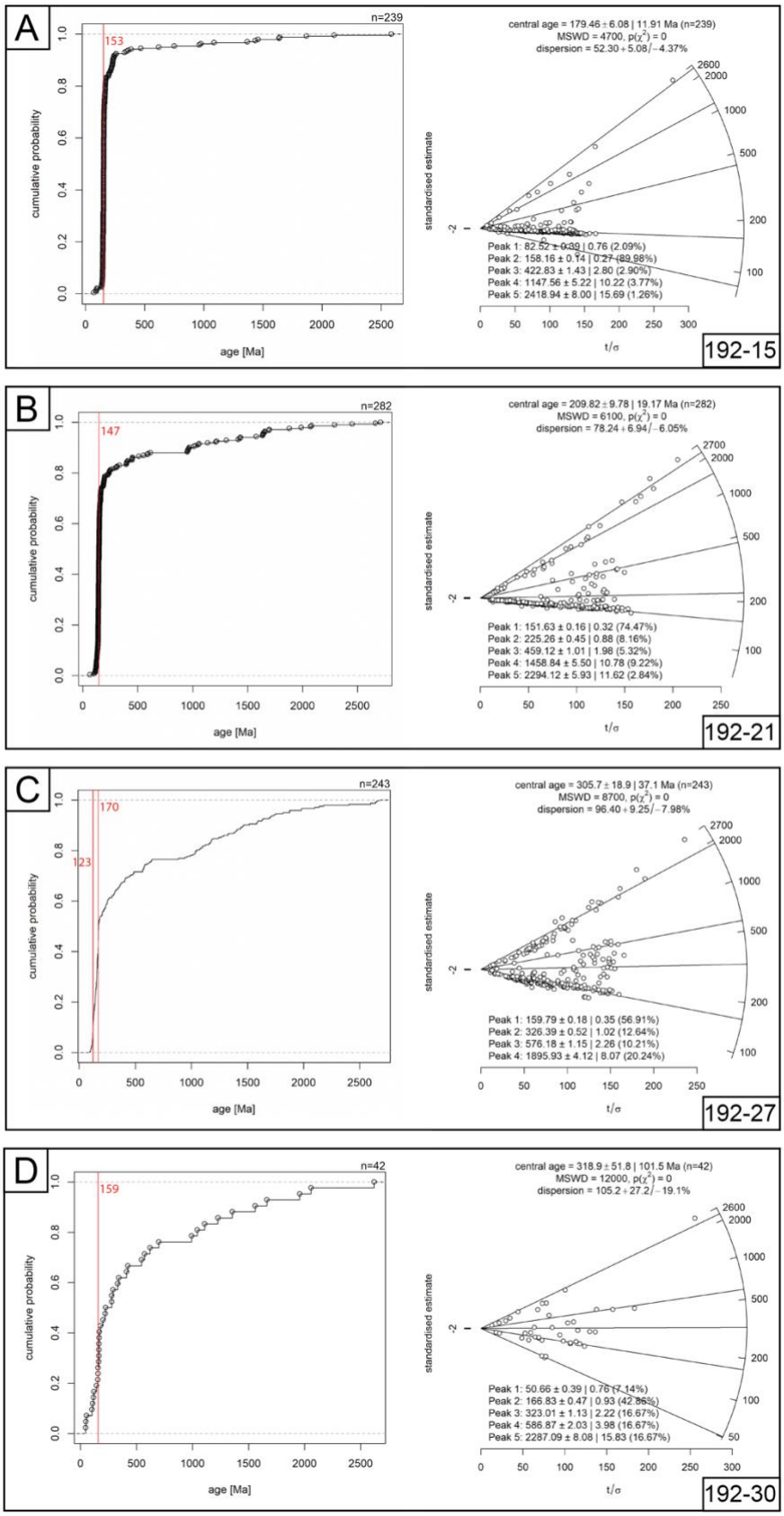
A
n=239
153
cumulative probability
age [Ma]
central age = 179.46 ± 6.08 | 11.91 Ma (n=239)
MSWD = 4700, p(χ²) = 0
dispersion = 52.30 + 5.08 / − 4.37%
standardised estimate
t/σ
Peak 1: 82.52 ± 0.39 | 0.76 (2.09%)
Peak 2: 158.16 ± 0.14 | 0.27 (89.98%)
Peak 3: 422.83 ± 1.43 | 2.80 (2.90%)
Peak 4: 1147.56 ± 5.22 | 10.22 (3.77%)
Peak 5: 2418.94 ± 8.00 | 15.69 (1.26%)
192-15
B
n=282
147
central age = 209.82 ± 9.78 | 19.17 Ma (n=282)
MSWD = 6100, p(χ²) = 0
dispersion = 78.24 + 6.94 / − 6.05%
Peak 1: 151.63 ± 0.16 | 0.32 (74.47%)
Peak 2: 225.26 ± 0.45 | 0.88 (8.16%)
Peak 3: 459.12 ± 1.01 | 1.98 (5.32%)
Peak 4: 1458.84 ± 5.50 | 10.78 (9.22%)
Peak 5: 2294.12 ± 5.93 | 11.62 (2.84%)
192-21
C
n=243
170
123
central age = 305.7 ± 18.9 | 37.1 Ma (n=243)
MSWD = 8700, p(χ²) = 0
dispersion = 96.40 + 9.25 / − 7.98%
Peak 1: 159.79 ± 0.18 | 0.35 (56.91%)
Peak 2: 326.39 ± 0.52 | 1.02 (12.64%)
Peak 3: 576.18 ± 1.15 | 2.26 (10.21%)
Peak 4: 1895.93 ± 4.12 | 8.07 (20.24%)
192-27
D
n=42
159
central age = 318.9 ± 51.8 | 101.5 Ma (n=42)
MSWD = 12000, p(χ²) = 0
dispersion = 105.2 + 27.2 / − 19.1%
Peak 1: 50.66 ± 0.39 | 0.76 (7.14%)
Peak 2: 166.83 ± 0.47 | 0.93 (42.86%)
Peak 3: 323.01 ± 1.13 | 2.22 (16.67%)
Peak 4: 586.87 ± 2.03 | 3.98 (16.67%)
Peak 5: 2287.09 ± 8.08 | 15.83 (16.67%)
192-30

Figure 13. Cumulative age distribution (CAD) plots on the left and radial plots on the right. Red lines on the CAD plot show the peak age for largest young peak in each sample, with the age also in red. A-C) Mt. Josephine samples 192-15, 192-21, 192-27, respectively. D) Shuksan greenschist sample 192-30.

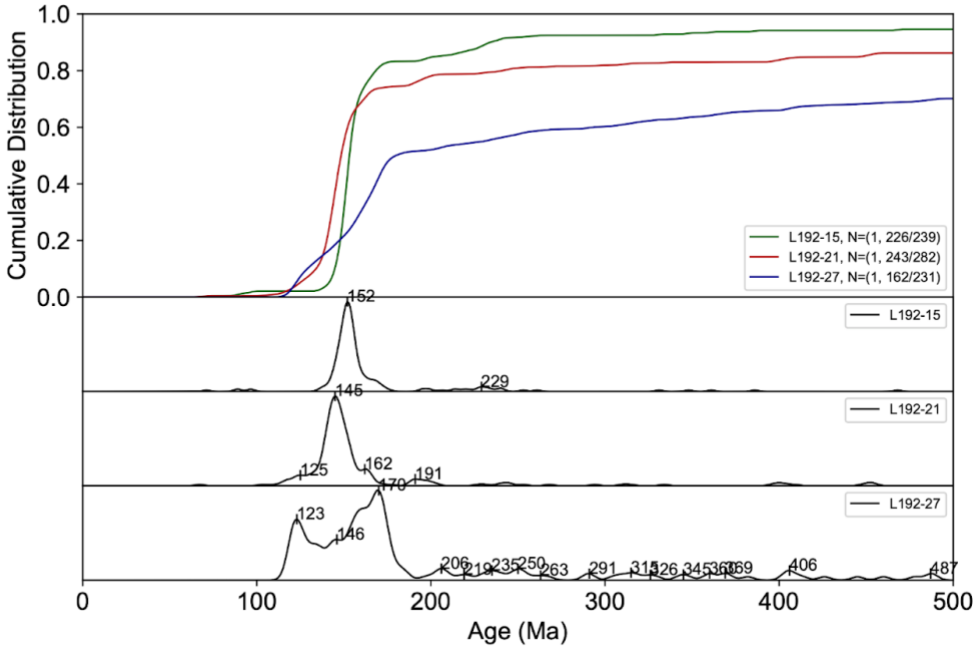

Figure 14. A stacked cumulative age distribution (CAD) plot and kernel density estimates (KDE) of the Mt. Josephine detrital samples with a high N using the detritalpy program. Sample number is to the right of each plot. Peak ages are labeled for the KDE plots.

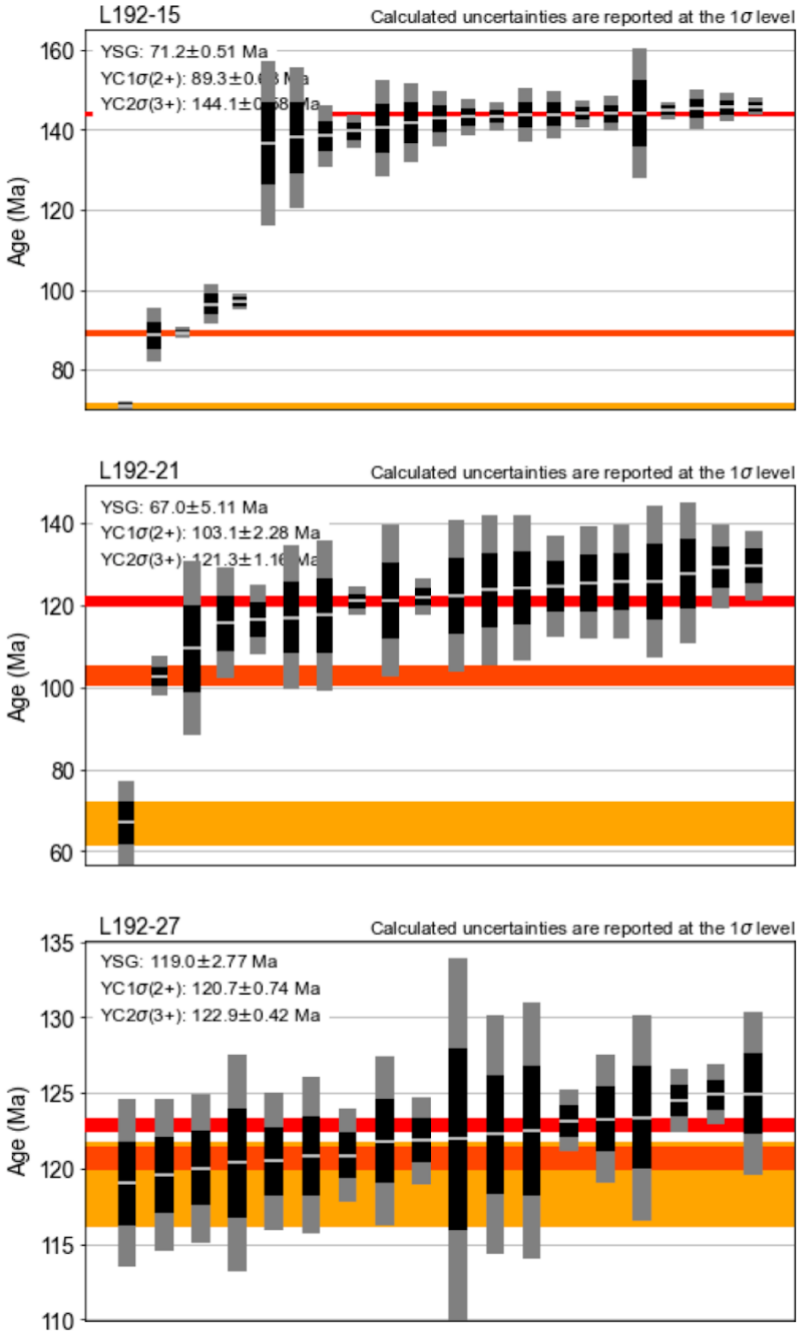

Figure 15. YC2σ(3+) plots showing the calculated maximum depositional ages (MDAs) from detritalpy of the three detrital samples in the Easton. Uncertainties reported at the 1σ level. YSG is the youngest single grain (light orange bar); YC1σ(2+) sorts all analyses by their U-Pb age plus 1σ uncertainty, and identifies the youngest cluster of analyses with overlapping 1σ error (orange bar); YC2σ(3+) sorts all analyses by their U-Pb age plus 2σ uncertainty, and identifies the youngest cluster of 3 or more analyses with overlapping 2σ error (red bar) (Sharman et al., 2018). Vertical black bars show 1σ uncertainty, gray bars show 2σ uncertainty.

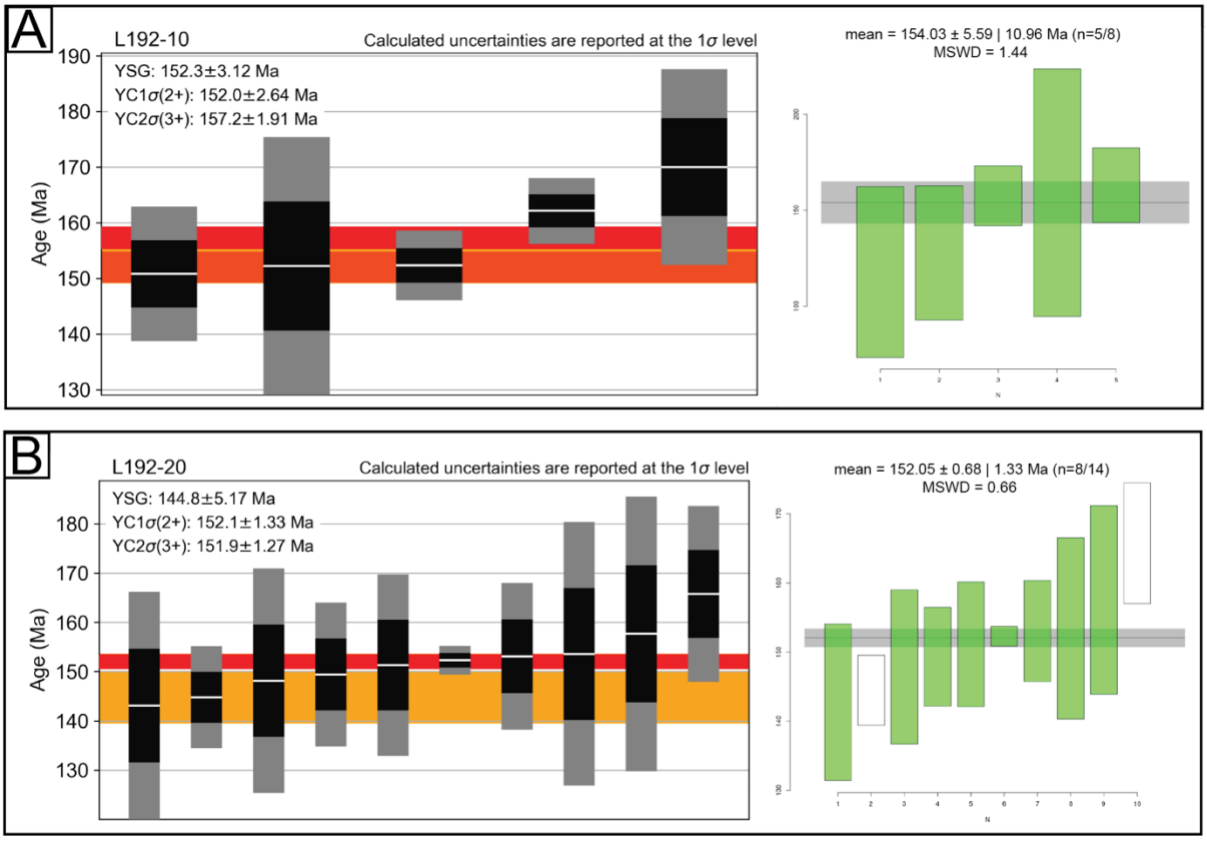

Figure 16. YC2σ(3+) plots showing the calculated maximum depositional ages (MDAs) from detritalpy and weighted mean plots of A) 192-10 (Mt. Josephine semi-schist, N=8) and B) 192-20 (Darrington phyllite, N=14), the two samples from this study with low zircon yields. For the weighted mean plots, the gray bar represents the weighted mean range, and is included for comparison to the YC2σ(3+) plots. The results at the top of the plot are reported as t ± x | y where t is the weighted mean age, x is the standard error, y is the 95% confidence interval (following Vermeesch, 2018). Individual ages plotted with 2σ errors.

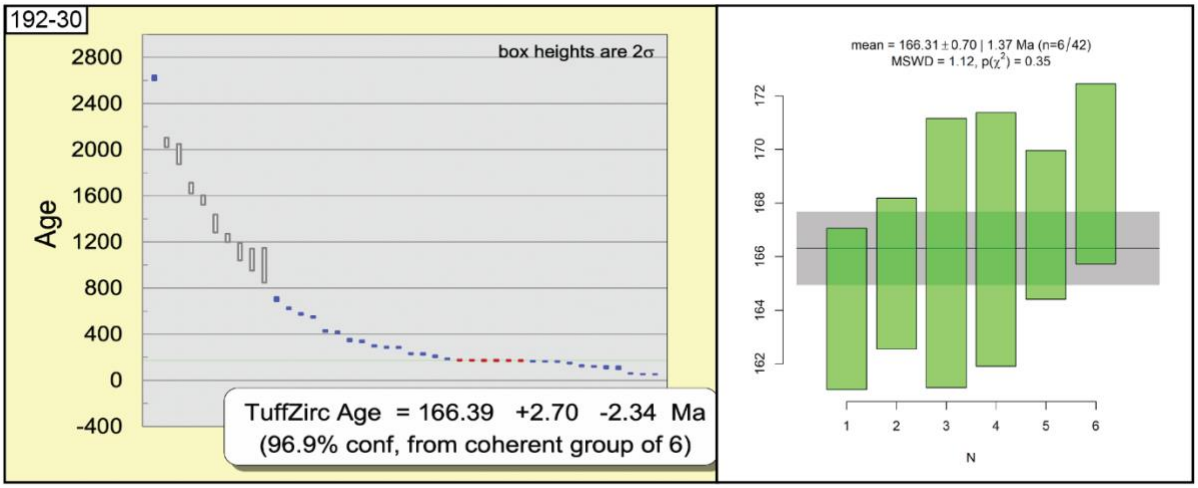

Figure 17. A TuffZirc plot and weighted mean plot of 192-30, the Shuksan greenschist sample. For the TuffZirc plots, methods follow Gehrels et al. (2008) and Gehrels and Pecha (2014). Red bars are analyses that are accepted, blue analyses are rejected; the TuffZirc age (green line) comes from the coherent group of red bars.

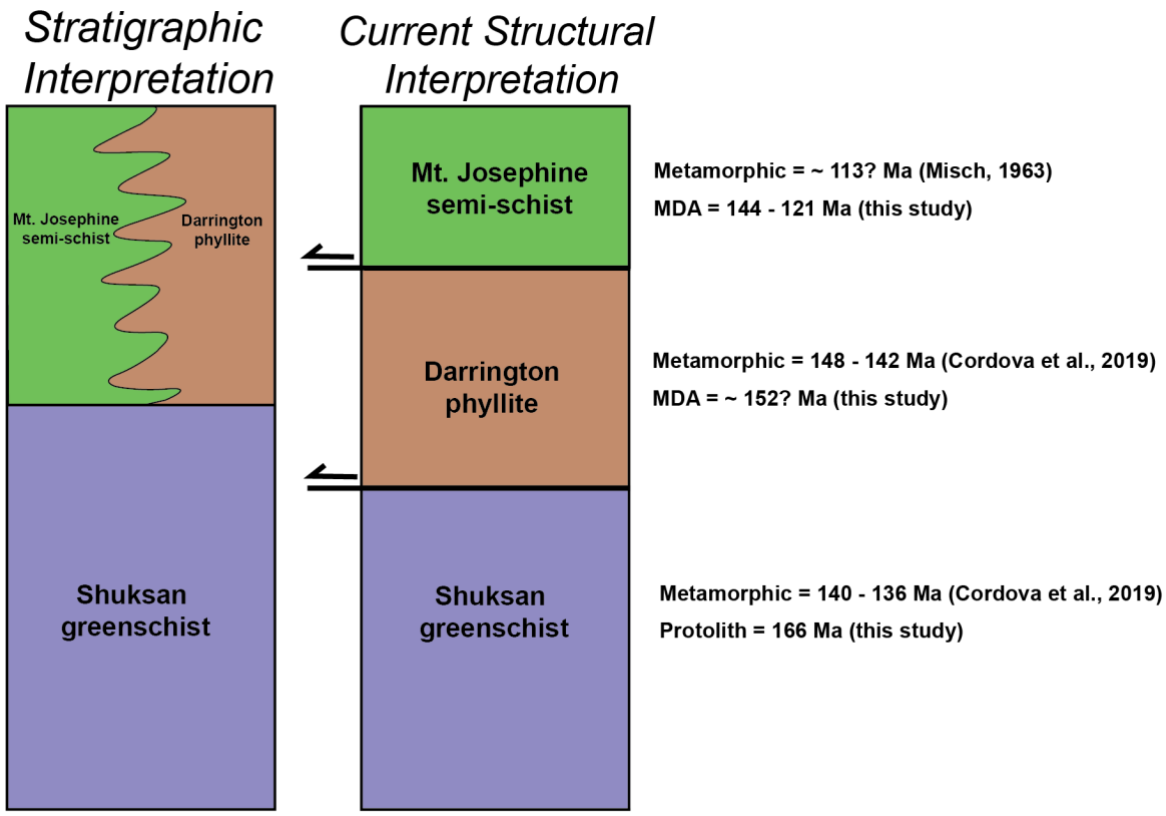

Figure 18. Stratigraphic columns of the current interpretations of the Easton metamorphic suite's regional blueschist units and the one proposed in this study. Metamorphic geochronology ages are from Misch (1963) and Cordova et al. (2019).

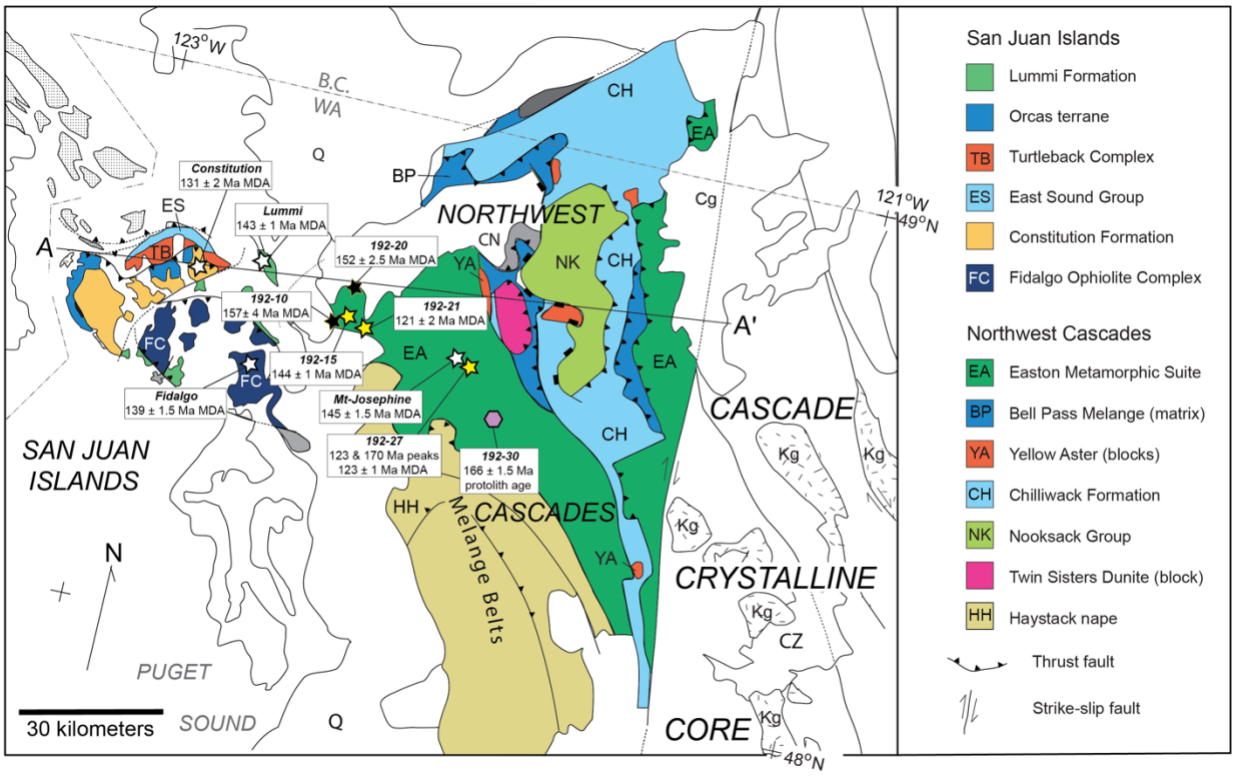

Figure 19. Geologic map and cross section of the Northwest Cascades Thrust System (NWCS) nappe sequence with U-Pb geochronology outlined. Yellow stars represent the Mt. Josephine maximum depositional ages (this study), the black stars represent Mt. Josephine and Darrington phyllite ages with low N (this study), the purple hexagon represents the Shuksan greenschist protolith age (this study), and the white stars represent previous U-Pb detrital zircon ages from comparable NWCS units in similar structural position (Brown and Gehrels, 2007). Bottom right shows a stacked age representation of the maximum depositional ages interpreted in text. Map modified from Brown and Gehrels (2007) and Schermer et al. (2018).

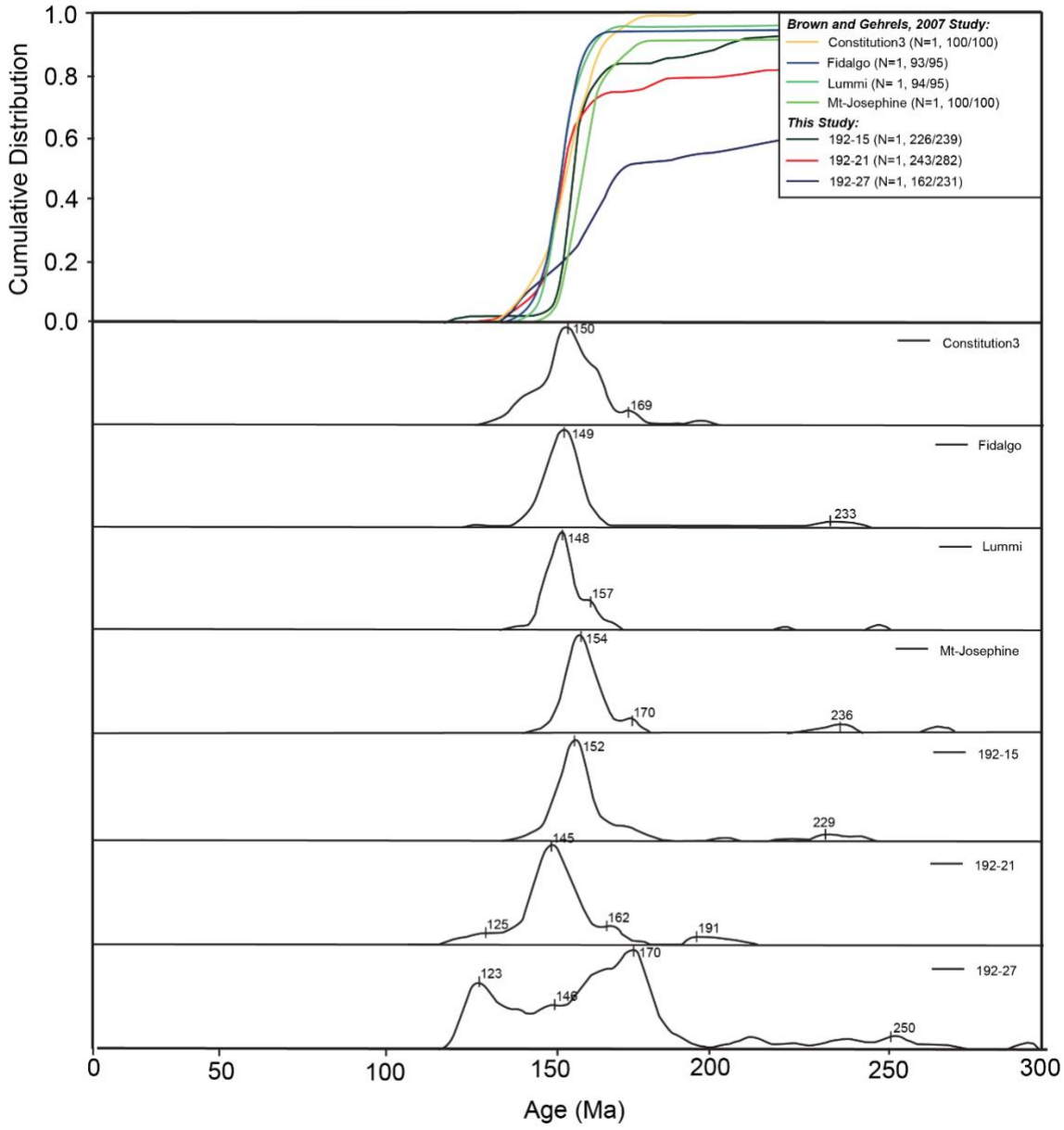

Figure 20. A stacked Cumulative Age Distribution (CAD) plot and Kernel Density Estimates (KDE) plot of the Constitution and Lummi Formations, Fidalgo Complex, and Mt. Josephine semi-schist within the Northwest Cascades System (NWCS), using the detritalpy program. Formation name is to the right of each plot. Peak ages are labeled for the KDE plots. Unit colors for Constitution, Fidalgo, and Lummi match those in Figure 19. Data from this study (192- samples) are from the Mt. Josephine semi-schist unit. All other NWCS data from Brown and Gehrels (2007).

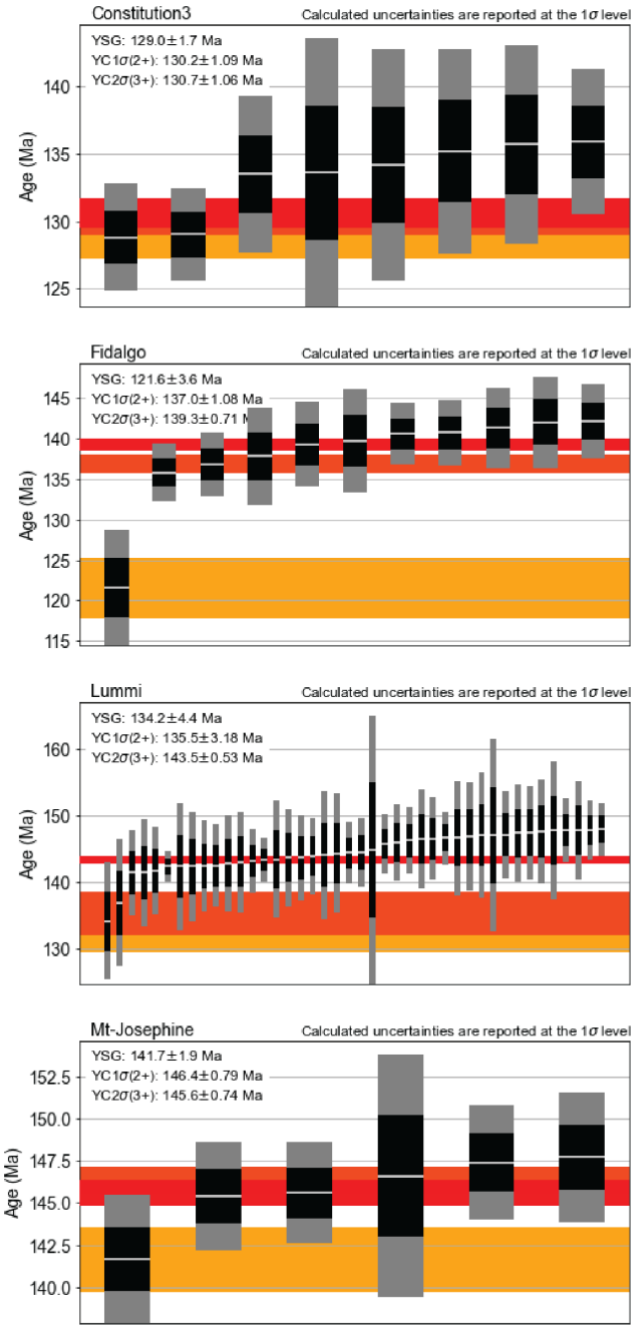

Figure 21. YC2σ(3+) weighted mean plots showing the maximum depositional ages (MDAs) from detritalpy of the Constitution and Lummi Formations, Fidalgo Complex, and Mt. Josephine semi-schist within the Northwest Cascades System (NWCS). Data from Brown and Gehrels (2007). Vertical black bars show 1σ uncertainty, gray bars show 2σ uncertainty. Calculated uncertainties on the plot are reported at the 1σ level.

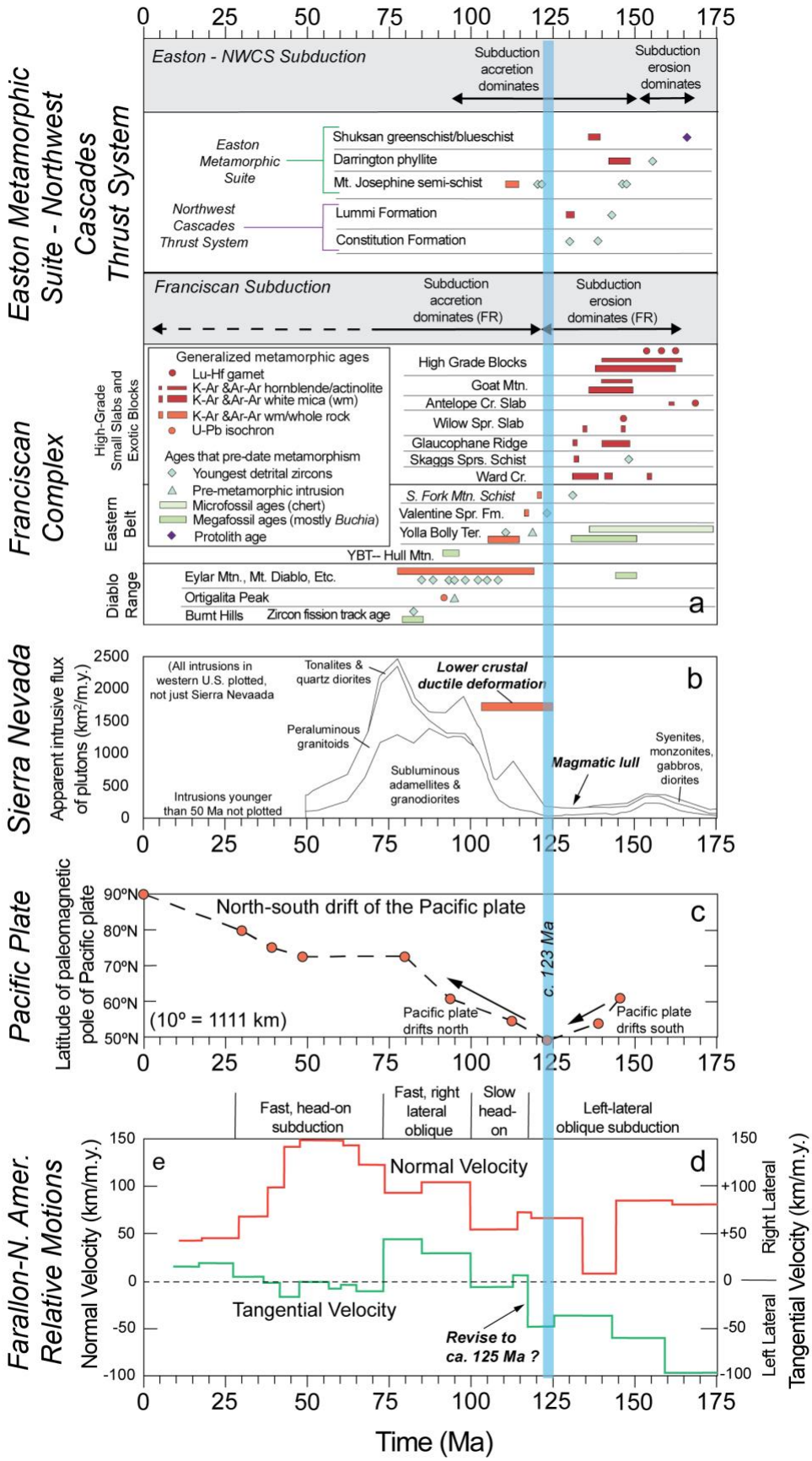
Easton Metamorphic Suite - Northwest Cascades Thrust System
Easton - NWCS Subduction
Subduction accretion dominates
Subduction erosion dominates
Easton Metamorphic Suite
Shuksan greenschist/blueschist
Darrington phyllite
Mt. Josephine semi-schist
Northwest Cascades Thrust System
Lummi Formation
Constitution Formation
Franciscan Subduction
Subduction accretion dominates (FR)
Subduction erosion dominates (FR)
Franciscan Complex
Generalized metamorphic ages
Lu-Hf garnet
K-Ar &Ar-Ar hornblende/actinolite
K-Ar &Ar-Ar white mica (wm)
K-Ar &Ar-Ar wm/whole rock
U-Pb isochron
Ages that pre-date metamorphism
Youngest detrital zircons
Pre-metamorphic intrusion
Microfossil ages (chert)
Megafossil ages (mostly Buchia)
Protolith age
High-Grade Small Slabs and Exotic Blocks
High Grade Blocks
Goat Mtn.
Antelope Cr. Slab
Wilow Spr. Slab
Glaucophane Ridge
Skaggs Sprs. Schist
Ward Cr.
Eastern Belt
S. Fork Mtn. Schist
Valentine Spr. Fm.
Yolla Bolly Ter.
YBT-- Hull Mtn.
Diablo Range
Eylar Mtn., Mt. Diablo, Etc.
Ortigalita Peak
Burnt Hills
Zircon fission track age
a
Sierra Nevada
Apparent intrusive flux of plutons (km²/m.y.)
(All intrusions in western U.S. plotted, not just Sierra Nevaada
Tonalites & quartz diorites
Lower crustal ductile deformation
Peraluminous granitoids
Subluminous adamellites & granodiorites
Magmatic lull
Syenites, monzonites, gabbros, diorites
Intrusions younger than 50 Ma not plotted
b
Pacific Plate
Latitude of paleomagnetic pole of Pacific plate
North-south drift of the Pacific plate
(10° = 1111 km)
Pacific plate drifts north
c. 123 Ma
Pacific plate drifts south
c
Farallon-N. Amer. Relative Motions
Fast, head-on subduction
Fast, right lateral oblique
Slow head-on
Left-lateral oblique subduction
Normal Velocity (km/m.y.)
Normal Velocity
Tangential Velocity
Revise to ca. 125 Ma ?
e
d
Right Lateral
Left Lateral
Tangential Velocity (km/m.y.)
Time (Ma)

Figure 22. Comparison of timing of events in the Franciscan subduction complex and the Easton metamorphic suite. Modified from Dumitru et al. (2010) to add the geochronology from this study into the regional subduction framework. Geochronologic data used in the Easton – NWCS section from this study, Misch (1963), Lamb (2000), Brown and Gehrels (2007), and Cordova et al. (2019). Note the ca. 123 Ma events in all diagrams (blue bar).

TABLES.

Table 1. Sample locations, unit names, and lithologies for geochronology samples.

Sample	Latitude	Longitude	Unit	Lithology
192-10	48.61425896	-122.441978	Mt. Josephine	semi-schist
192-15	48.61754802	-122.419904	Mt. Josephine	semi-schist
192-20	48.66593599	-122.412255	Darrington	phyllite
192-21	48.60687702	-122.35734	Mt. Josephine	semi-schist
192-27	48.57564798	-121.970637	Mt. Josephine	graphitic semi-schist
192-30	48.48114897	-121.935403	Shuksan	meta-tuff

Table 2. Geochronology samples, zircon yields, reported age types, and ages from this study.

Sample	Unit	High/Low N	Geochronology	Reported Age Type	Age
192-10	Mt. Josephine	Low N	Detrital Zircon	YC2σ(3+)	157.2 ± 3.82 Ma MDA
192-15	Mt. Josephine	High N	Detrital Zircon	YC2σ(3+)	144.1 ± 1.16 Ma MDA
192-20	Darrington	Low N	Detrital Zircon	YC2σ(3+)	151.9 ± 2.54 Ma MDA
192-21	Mt. Josephine	High N	Detrital Zircon	YC2σ(3+)	121.3 ± 2.32 Ma MDA
192-27	Mt. Josephine	High N	Detrital Zircon	YC2σ(3+)	122.9 ± 0.84 Ma MDA
192-30	Shuksan	High N	Igneous Zircon	Weighted Mean	166.31 ± 1.37 Ma